Prospects for the measurement of the structure of the coupling of a Higgs boson to weak gauge bosons in weak boson fusion with the ATLAS detector

C. Ruwiedel[1,a], M. Schumacher[2], N. Wermes[1]

[1] Physikalisches Institut, Universität Bonn, Nussallee 12, 53115 Bonn, Germany
[2] Fachbereich Physik, Universität Siegen, Siegen, Germany

Abstract. The prospects for the measurement of the tensor structure of the vertex between a standard model Higgs boson and two weak gauge bosons using the distribution of the azimuthal angles between the two tagging jets in the weak boson fusion channel are studied in a Monte Carlo analysis using the fast simulation of the ATLAS detector. The decay channels $H \to \tau^+\tau^- \to ll + 4\nu$, $H \to \tau^+\tau^- \to lh + 3\nu$ at $m_H = 120$ GeV and $H \to W^+W^- \to ll\nu\nu$ at $m_H = 160$ GeV are used in the analysis. For a standard model Higgs boson it is found that purely anomalous couplings are expected to be excluded at a confidence level corresponding to 2σ or more at $m_H = 120$ GeV and more than 5σ at $m_H = 160$ GeV from 30 fb^{-1} of data. With a value of 1 roughly reproducing the standard model cross section for a purely anomalous coupling, the standard deviation in a measurement of a contribution of a CP even anomalous coupling in addition to the standard model coupling is estimated to be 0.20 at $m_H = 120$ GeV and 0.09 at $m_H = 160$ GeV.

1 Introduction

One of the main purposes of the ATLAS experiment is the investigation of the predicted effects of electroweak symmetry breaking and the description of particle masses in the standard model. Monte Carlo studies of the discovery potential for a standard model Higgs boson, which is a necessary component of the symmetry breaking mechanism of the standard model, indicate that it will be possible to discover the Higgs boson, if it exists, over the whole mass range which is not yet excluded from measurements of the electroweak sector. One of the most promising channels for the discovery of a Higgs boson is the weak boson fusion channel [1].

After the discovery of a new particle at the LHC the question will arise what kind of particle it is. Thus, in a next step, its quantum numbers and couplings will be investigated. It has been proposed [2] to use the distribution of the azimuthal angles between the tagging jets in weak boson fusion to determine the structure of the coupling of a scalar Higgs particle candidate to two weak bosons. For simplicity, the scalar particle under study will sometimes just be called Higgs boson in the following. The potential for this measurement with the ATLAS detector is studied using the fast detector simulation ATLFAST. The angular correlations that are used are largely independent of the mass and decay channel of the Higgs boson. Thus, the analysis can be performed for differ-

ent decay channels and Higgs boson masses in a similar way.

In addition to the standard model coupling of a Higgs boson to weak gauge bosons anomalous couplings arising from terms in an effective Lagrangian are considered. A measurement of the anomalous couplings can provide information about the CP quantum number of the Higgs boson and about possible loop contributions to the coupling from particles with large mass.

The structure of the coupling vertex with standard model and anomalous contributions is discussed in Sect. 2. The present experimental limits on the anomalous couplings from measurements at LEP and especially the L3 experiment are given in Sect. 2.2.

Event generation and event selection are discussed in Sects. 3 and 4.

The first of two parts of the analysis, an investigation of the prospects for the determination of the dominant coupling term, is presented in Sect. 5. This measurement can be used to determine the CP quantum number of the scalar particle and it can be used to decide whether the coupling is loop-induced or standard model-like. The case of a standard model Higgs boson for which anomalous couplings are to be excluded is studied as a reference case in this section.

In the second part of the analysis the sensitivity of the ATLAS experiment to a contribution by an anomalous coupling in addition to the standard model coupling is estimated using a likelihood fit. The results of this analysis are presented in Sect. 6.

This note is based on the results of [3] (in German).

a e-mail: ruwiedel@physik.uni-bonn.de

2 Anomalous Higgs boson couplings

Deviations from the predictions of the standard model for the couplings of a Higgs boson to weak gauge bosons are parametrised in a systematic and model-independent way in an effective, gauge invariant Lagrangian. This effective Lagrangian contains terms composed of Higgs and weak gauge fields with mass dimension higher than 4. A theory containing such terms is not renormalisable. It is considered an effective theory that is valid only up to a certain energy scale Λ where it has to be replaced by a more fundamental theory containing new particles. An effective Lagrangian is often written as an expansion in $1/\Lambda$:

$$\mathcal{L}_{\text{eff}} = \mathcal{L}_{\text{SM}} + \sum_i \frac{g_i^{(5)}}{\Lambda} \mathcal{O}_i^{(5)} + \sum_i \frac{g_i^{(6)}}{\Lambda^2} \mathcal{O}_i^{(6)} + \dots \quad (1)$$

In this expansion the operators are ordered by their dimension and are assumed to contribute less the higher their dimension is. The g_i are dimensionless coupling constants with a magnitude of the order of 1. A comprehensive list of operators of up to dimension 6 is given in [4]. In this study, the following operators are considered, as given in [5]:

$$\mathcal{L}_5 = \frac{g_{5e}^{HWW}}{\Lambda_{5e}} H W_{\mu\nu}^+ W^{-\mu\nu} + \frac{g_{5o}^{HWW}}{\Lambda_{5o}} H \tilde{W}_{\mu\nu}^+ W^{-\mu\nu}$$
$$+ \frac{g_{5e}^{HZZ}}{2\Lambda_{5e}} H Z_{\mu\nu} Z^{\mu\nu} + \frac{g_{5o}^{HZZ}}{2\Lambda_{5o}} H \tilde{Z}_{\mu\nu} Z^{\mu\nu} . \quad (2)$$

The dimension 5 operators in (2) arise from dimension 6 operators of the structure $(\Phi^\dagger\Phi)V_{\mu\nu}V^{\mu\nu}$ and $(\Phi^\dagger\Phi)\tilde{V}_{\mu\nu}V^{\mu\nu}$, with $V = W/Z$, when the Higgs field is written in its physical expansion,

$$\phi = \frac{1}{\sqrt{2}} \begin{pmatrix} 0 \\ v + H(x) \end{pmatrix} . \quad (3)$$

The field strength tensor $V^{\mu\nu}$ of the field V is even under CP transformations while the dual field strength tensor, given by

$$\tilde{V}^{\mu\nu} = \frac{1}{2}\epsilon^{\mu\nu\rho\sigma}V_{\rho\sigma} , \quad (4)$$

is CP odd.

As long as the field H in (2) is the standard model Higgs boson field, which is CP even, the operators composed of the field strength tensors are CP even, indicated by the subscript e on the coupling constant g and the scale Λ, while the operators containing the dual field strength tensors are CP odd, indicated by the subscript o. In a CP conserving theory only the CP even operators will contribute to the coupling. In more general models with additional scalar particles the effective Lagrangian in (2) may be used to describe the couplings of those scalar particles to weak gauge bosons. If in this case H represents a CP odd scalar particle, the operators will switch their behaviour under CP transformations. The operators containing the dual field strength tensors will now be CP even and give the only contribution to the coupling if CP is conserved.

Thus, assuming CP conservation it is possible to determine the CP quantum number of the scalar particle by experimentally distinguishing between the coupling terms. This is one of the goals of the analysis presented in Sect. 5.

The vertex that couples a Higgs boson to vector bosons is written in its most general form as [5]:

$$T^{\mu\nu}(q_1, q_2) = a_1(q_1, q_2) g^{\mu\nu}$$
$$+ a_2(q_1, q_2) [q_1 \cdot q_2 g^{\mu\nu} - q_2^\mu q_1^\nu]$$
$$+ a_3(q_1, q_2) \epsilon^{\mu\nu\rho\sigma} q_{1\rho} q_{2\sigma} \quad (5)$$

with the four-momenta of the vector bosons q_1 and q_2. The $a_i(q_1, q_2)$ are Lorentz-invariant form factors. In the standard model at leading order, the only non-vanishing coefficient is given by:

$$a_1(q_1, q_2) = \frac{2m_V^2}{v} . \quad (6)$$

The effective Lagrangian of (2) gives the additional couplings

$$a_2(q_1, q_2) = -\frac{2}{\Lambda_{5e}} g_{5e}^{HWW}$$
$$a_3(q_1, q_2) = \frac{2}{\Lambda_{5o}} g_{5o}^{HWW} \quad (7)$$

for the HWW vertex and

$$a_2(q_1, q_2) = -\frac{2}{\Lambda_{5e}} g_{5e}^{HZZ}$$
$$a_3(q_1, q_2) = \frac{2}{\Lambda_{5o}} g_{5o}^{HZZ} \quad (8)$$

for the HZZ vertex.

As in [5], the ratio of the anomalous HWW couplings to the anomalous HZZ couplings is chosen according to $g_{5e/o}^{HWW} = g_{5e/o}^{HZZ} \cos^2\theta_w$ in this analysis which corresponds to a ratio equal to that of the respective standard model couplings. The scale $\Lambda_{5e/o}$ is fixed, as in [5], to a value of 480 GeV which roughly reproduces the standard model cross section for weak boson fusion at a Higgs boson mass of 120 GeV and for a purely anomalous CP even or a purely anomalous CP odd coupling with

$$g_{5e/o}^{HWW} = g_{5e/o}^{HZZ} \cos^2\theta_w = 1 .$$

This leaves two free parameters, e.g. g_{5e}^{HZZ} and g_{5o}^{HZZ}, which define the strength of the anomalous couplings.

2.1 Examples for anomalous Higgs-vector boson couplings

A well-known example for the occurrence of the CP even anomalous coupling is the production of a Higgs boson in the standard model through gluon–gluon–fusion, which is mediated by a top quark-dominated loop. In the limit of a large top quark mass the vertex is of the form $T^{\mu\nu} \propto (q_1 \cdot q_2 g^{\mu\nu} - q_1^\nu q_2^\mu)$ with the momenta of the gluons q_1 and q_2. The similar loop-induced contribution to the coupling

of a Higgs boson to weak bosons in the standard model is suppressed by a factor of $\alpha_W/\pi \approx 10^{-2}$ [2]. It will be shown in Sect. 6 that a contribution of this size will not be observable at the LHC.

The CP odd A^0 Higgs boson of the minimal supersymmetric standard model does not couple to weak bosons at leading order. There is an anomalous loop-induced coupling of the form $A^0 \tilde{V}_{\mu\nu} V^{\mu\nu}$ which, however, will be too weak to be observable at the LHC. The effective coupling of a top-pion, which occurs in topcolor models, to weak bosons is cited in [2] as an example of a coupling described by the operators containing the dual field strength tensors which may lead to an observable event rate at the LHC.

2.2 Experimental limits on the anomalous couplings

The possibility of a contribution of a CP even anomalous coupling of a Higgs boson to weak gauge bosons in addition to the standard model coupling has been studied at LEP by the L3 collaboration. The resulting limits on the couplings have been published in [6]. In the parametrisation of the L3 collaboration, the relevant part of the effective Lagrangian is:

$$\mathcal{L}_{\text{eff}} = g^{(1)}_{HWW}(W^+_{\mu\nu} W^{\mu}_- \partial^\nu H + h.c.)$$
$$+ g^{(2)}_{HWW} H W^+_{\mu\nu} W^{\mu\nu}_- + g^{(1)}_{HZZ} Z_{\mu\nu} Z^\mu \partial^\nu H$$
$$+ g^{(2)}_{HZZ} H Z_{\mu\nu} Z^{\mu\nu} , \quad (9)$$

where

$$g^{(1)}_{HWW} = \frac{g\, m_W}{m_Z^2} \Delta g_1^Z \quad (10)$$

$$g^{(2)}_{HWW} = \frac{g}{m_W} d \quad (11)$$

$$g^{(1)}_{HZZ} = \frac{g}{m_W} \left(\Delta g_1^Z \cos 2\theta_W + \Delta\kappa_\gamma \tan^2\theta_W \right) \quad (12)$$

$$g^{(2)}_{HZZ} = \frac{g}{2m_W} \left(d \cos^2\theta_W + d_B \sin^2\theta_W \right) . \quad (13)$$

All of the terms in (9) give contributions to the CP even anomalous coupling a_2 of equation (5) even though in this parametrisation not all of the terms are of the form $HV_{\mu\nu}V^{\mu\nu}$. Limits on CP odd anomalous couplings were not determined in the L3 study.

The limits on the parameters d and d_B from the L3 study are given as the 95% confidence level contour plots shown in Fig. 1. For the Higgs boson mass values used in this analysis the limits were read from the plots and collected in Table 1. The parameters Δg_1^Z and $\Delta\kappa_\gamma$ also appear in parametrisations of deviations from the standard model triple gauge boson couplings and the best limits were established from measurements of triple gauge boson couplings by all four LEP experiments. The limits on these parameters were determined from values published in [23] and collected in Table 2.

Values of the parameters d, d_B, Δg_1^Z and $\Delta\kappa_\gamma$ are converted to corresponding values of the parameters g_{5e}^{HWW} and g_{5e}^{HZZ} of (2) using the following conversion rules from the program vbfnlo (see Sect. 3.1):

$$g_{5e}^{HWW} = \Lambda_{5e} \frac{g}{m_W} \left(d + \Delta g_1^Z \frac{m_W^2}{m_Z^2} \right) \quad (14)$$

$$g_{5e}^{HZZ} = \Lambda_{5e} \frac{g}{m_W} (d \cos^2\theta_W + d_B \sin^2\theta_W$$
$$+ \Delta g_1^Z \cos 2\theta_W + \Delta\kappa_\gamma \tan^2\theta_W) . \quad (15)$$

Rough estimates of 95% confidence level intervals for the parameters g_{5e}^{HWW} and g_{5e}^{HZZ} were determined by using error propagation in (14) and (15) which implies the assumption that the parameters d, d_B, Δg_1^Z and $\Delta\kappa_\gamma$ are uncorrelated and distributed according to Gaussian distributions around the central values of the confidence intervals. If the parameters are correlated to some degree the approximation should still be reasonable because the resulting limits are dominated by the uncertainty on the parameter d. For the purpose of comparing the results of this study to the limits from the L3 analysis the calculated limits can be regarded as conservative in the sense that

Exclusion (95% CL):

- Combined — ☒ ee→γγγ, eeγγ — ☒ ee→HZ
- -- Expected limit — ☰ ee→Zγγ — ☒ ee→WW$^{(*)}$γ
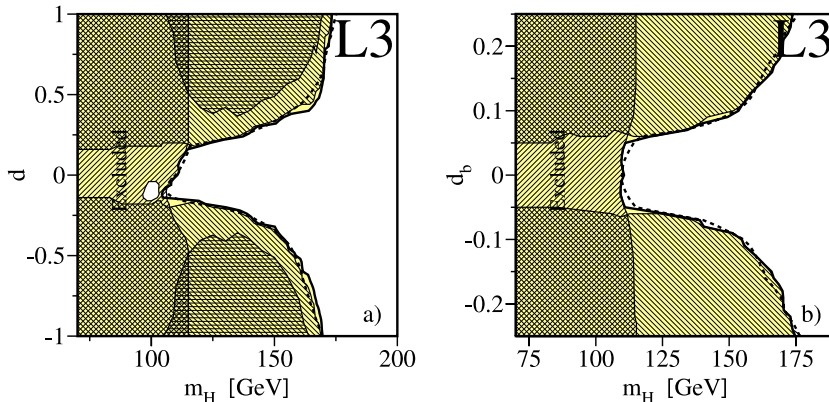
Fig. 1. 95% confidence level (CL) exclusion limits on the parameters d and d_B as published by the L3 collaboration [6]

Table 1. 95% confidence level intervals for the parameters d and d_B, determined from the plots in Fig. 1

m_H	d	d_B
120 GeV	$-0.19 \ldots 0.19$	$-0.06 \ldots 0.06$
160 GeV	$-0.50 \ldots 0.40$	$-0.13 \ldots 0.14$

Table 2. 95% confidence level intervals for the parameters Δg_1^Z and $\Delta \kappa_\gamma$, taken from [23]

Δg_1^Z	$\Delta \kappa_\gamma$
$-0.051 \ldots 0.034$	$-0.105 \ldots 0.069$

Table 3. Approximate 95% confidence level intervals for the parameters g_{5e}^{HWW} and g_{5e}^{HZZ}, calculated from the values in Tables 1 and 2 (see text)

m_H	g_{5e}^{HWW}	g_{5e}^{HZZ}
120 GeV	$-0.78 \ldots 0.73$	$-0.63 \ldots 0.55$
160 GeV	$-2.0 \ldots 1.5$	$-1.6 \ldots 1.3$

they may overestimate the sensitivity of the L3 study. The limits are given in Table 3.

One can see from the values given in Table 3 that the limits on the Higgs boson coupling to W boson pairs are slightly weaker than the limits on the coupling to Z boson pairs. One can also see from Fig. 1 and from Tables 1 and 3 that the limits on the anomalous couplings get weaker as the Higgs boson mass increases.

3 Event generation

Events for some of the processes used in this study were generated with parton level event generators while others were generated with Pythia. The events from the parton level generators were passed to the ATLAS software framework ATHENA using data files containing the information from the Les Houches common blocks [7]. Parton shower, fragmentation, hadron decays, underlying event, τ lepton decays, final state electromagnetic radiation from τ leptons and the detector simulation were calculated for all processes with Pythia 6.226 [8], Tauola 2.7 [9], Photos 2.6 [10] and ATLFAST [11] respectively. Version 10.0.1 of ATHENA was used. The version of ATLFAST used in ATHENA 10.0.1 has not been formally validated within the ATLAS collaboration and, albeit being considered as appropriate for this study, results obtained using this version cannot be compared directly to other ATLAS results. In all programs the parton density functions CTEQ5L [12] were used.

For the reconstruction of jets in ATLFAST a basic simulation of the calorimeter is used. Particle energies are summed in cells from which then clusters are formed fol-

lowing a cone-based method with a cone radius of $\Delta R^1 = 0.4$. The energies of the clusters are then modified using a Gaussian energy resolution function, followed by several additional steps, to obtain jets. A detailed description of the detector simulation and reconstruction with ATLFAST is given in [11]. For the minimum transverse energy threshold for clusters and for the minimum transverse momentum threshold for isolated photons the default values in ATHENA 10.0.1 were used which are both 5 GeV. These values differ from the ones in [11].

3.1 Signal events

Signal events for the weak boson fusion process were generated with the program vbfnlo [13] which contains the anomalous Higgs boson couplings described in the previous section. In the version of vbfnlo used in this study, unweighted events can only be generated at leading order, hence the program was used at leading order. The version of vbfnlo used in this study does not assign spins and masses to the final-state τ leptons. They were added by modifying the event data files, following a prescription provided by the author of the program [14].

When generating events with vbfnlo one has to take care that the "scale of the event", which is stored in the Les Houches variable SCALUP, is set to a suitable value. If the scale of the event is not set, indicated by a value of the variable SCALUP of -1, Pythia uses the centre-of-mass energy of the parton-parton system $\hat{s}$ which is generally considered too large in weak boson fusion. In this study, the factorisation and renormalisation scales in vbfnlo were set for each quark line to the momentum transfer of the corresponding W or Z boson. In the Les Houches file, the variable SCALUP was set to the W boson mass for WW fusion events and to the Z boson mass for ZZ fusion events.

When using parton-level events generated by an external generator, the value of SCALUP is multiplied in Pythia by the parameter PARP(67) to determine the cut-off scale for the initial-state parton shower and by the parameter PARP(71) to determine the cut-off scale for the final-state parton shower. These multiplicative factors are not applied when the weak boson fusion events are generated by Pythia itself. To achieve consistency between the results from events generated with vbfnlo when used with standard model couplings and those from events generated with Pythia, the parameter PARP(71) was changed from the default value of 4 in ATHENA 10.0.1 to 1 while for the parameter PARP(67) the default value of 1 was kept. The results from Pythia are compared to the results from vbfnlo with standard model couplings in Sect. 4.6 after the discussion of the event selection.

Signal events were generated for the Higgs boson decay channels $H \to \tau^+ \tau^- \to ll + 4\nu$ and $H \to \tau^+ \tau^- \to lh + 3\nu$ at a Higgs boson mass of 120 GeV and for the Higgs boson decay channel $H \to W^+ W^- \to ll\nu\nu$ at a Higgs boson mass of 160 GeV. In the channel $H \to \tau^+ \tau^- \to ll + 4\nu$

---

[1] $\Delta R = \sqrt{\Delta \eta^2 + \Delta \phi^2}$ is a measure of the distance in the η-ϕ-plane.

only leptonic decay modes were allowed for the decays of both τ leptons while in the channel $H \to \tau^+\tau^- \to lh + 3\nu$ only leptonic decay modes were allowed for the decay of one τ lepton and only hadronic decay modes, with all possible multiplicities of charged hadrons, were allowed for the decay of the other τ lepton. According to the analyses at leading order of the discovery potential for a standard model Higgs boson with the ATLAS detector (see Fig. 2) those are the channels with the highest expected signal significances at the respective Higgs boson masses. The mass values are chosen to lie within the region which has not yet been experimentally excluded for a standard model Higgs boson.

For each channel 4.5 million events were generated with standard model (SM) couplings. In addition, for each channel 1.5 million events with purely CP even anomalous couplings ($g_{5e}^{HZZ} = g_{5e}^{HWW} / \cos^2 \theta_w = 1$, "CPE") and 1.5 million events with purely CP odd anomalous couplings ($g_{5o}^{HZZ} = g_{5o}^{HWW} / \cos^2 \theta_w = 1$, "CPO") were generated. In these samples the standard model couplings were set to 0. The cross sections for the standard model case were taken from [1]. The cross sections for the samples with purely anomalous couplings depend directly on the undetermined strengths of the anomalous couplings. Since these samples are used in a hypothesis test in which only the shape of a distribution is tested, no a priori assumption about the total cross sections was made.

3.2 Background events

– Events in which the Higgs boson is produced by gluon–gluon–fusion were generated for each signal channel with Pythia. This process is listed as a background process here because the focus of this study is not the discovery potential for a Higgs boson but rather the determination of the couplings of the Higgs boson to weak bosons, to which gluon–gluon–fusion does not contribute. This labelling has no effect on the treatment
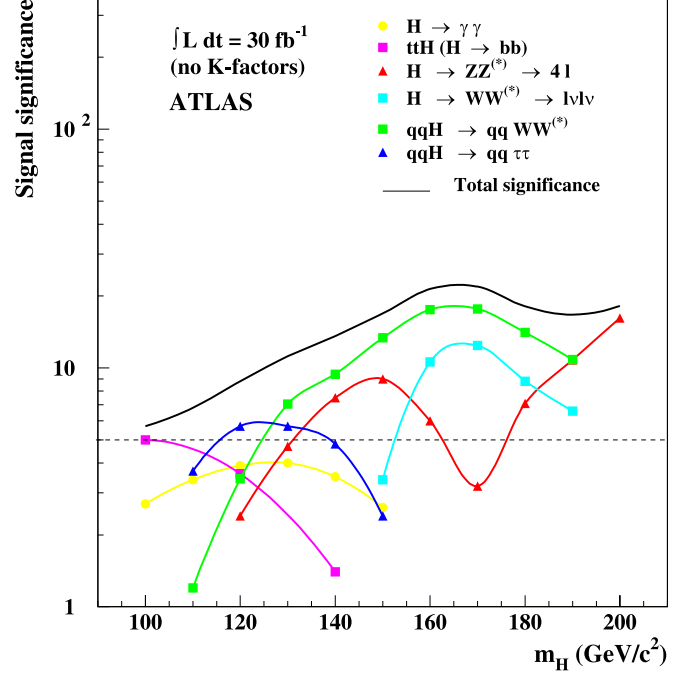
Fig. 2. Expected signal significance with the ATLAS experiment for a standard model Higgs boson in the region of small to intermediate Higgs boson masses [1]

of this process in the analysis. For the calculation of the expected signal significance in Sect. 4 the process is nevertheless treated as part of the signal to facilitate comparison with studies of the discovery potential where this convention is generally used.

– $t\bar{t}$ events were generated with Pythia. In this event sample W bosons were forced to decay leptonically.

– Wt events were generated with TopReX 4.06 [15]. All decay channels were allowed. A filter was applied to the generated events that required at least one lepton with $|\eta| < 3$ and $p_T > 8$ GeV.

Table 4. Cuts applied at the generator level (i.e. at parton level). For Monte Carlo events generated with Pythia and TopReX the standard settings of Pythia and TopReX in ATHENA 10.0.1 were used

	WBF	$WWjj$(EW)	$WWjj$(QCD)	Zjj(EW)	Zjj(QCD)
all final state quarks:					
p_T	> 5 GeV	> 15 GeV	> 15 GeV	> 5 GeV	> 20 GeV
E	> 5 GeV	–	–	–	–
$|\eta|$	–	< 5.5	< 6	–	< 6
ΔR	–	> 0.3	–	–	–
$|\Delta\eta|$	–	–	–	–	> 3
m_{qq}	–	–	> 200 GeV	–	> 400 GeV
all final state leptons:					
p_T	–	–	–	> 5 GeV	> 5 GeV
$|\eta|$	–	–	–	–	< 3
m_{ll}	–	–	–	(76.19–251.19) GeV	(75–160) GeV
all quarks and leptons:					
ΔR_{ql}	–	–	–	–	> 0.3

– $WWjj$ events from electroweak production were generated with MadEvent [16]. The decays of the W bosons were calculated with Pythia. Only leptonic decay modes were allowed. For consistency with the signal event generation the parameter PARP(71) in Pythia was set to 1.

– $WWjj$ events from QCD production were generated with MadEvent [16]. Again, for the W bosons only leptonic decay modes were allowed. Because of technical problems with Pythia in ATHENA 10.0.1 the decays were calculated with MadEvent for this process. Since this is a QCD process the parameter PARP(71) was left at its default value.

– Zjj events from electroweak and from QCD production were generated with MadCUP which is based on calculations presented in [17, 18] and references therein.

Leptonic decays of the Z boson were calculated by MadCUP.

An overview of the cuts applied at the generator level is given in Table 4. A list of all generated Monte Carlo samples is given in Table 5.

4 Event selection

Events are selected following the cut analyses described in [1] which are optimised to give the maximum signal significance. In the following some selection criteria are motivated and lists of the cuts are given. Details about the cut analyses can be found in [1] and references therein. Some cuts are modified in the channel $H \to \tau^+\tau^- \to ll + 4\nu$

Table 5. List of the generated Monte Carlo event samples. The statistical errors on the cross sections are known and non-negligible only for the processes WWjj(EW) and WWjj(QCD). The cross sections of the signal processes and the branching ratios for the Higgs boson decays were taken from [1]. Branching ratios for the W boson decays were taken from [19]. The cross sections that are given for background processes are those calculated by the respective programs with the cuts at generator level as given in Table 4. For the case of purely anomalous couplings no cross sections were calculated

process	generator	cross section	number of events
WBF: $H \to \tau^+\tau^- \to ll + 4\nu$ $m_{\mathrm{H}} = 120$ GeV, SM couplings	vbfnlo	37.67 fb	4 500 000
WBF: $H \to \tau^+\tau^- \to ll + 4\nu$ $m_{\mathrm{H}} = 120$ GeV, CPE couplings	vbfnlo	–	1 500 000
WBF: $H \to \tau^+\tau^- \to ll + 4\nu$ $m_{\mathrm{H}} = 120$ GeV, CPO couplings	vbfnlo	–	1 500 000
WBF: $H \to \tau^+\tau^- \to lh + 3\nu$ $m_{\mathrm{H}} = 120$ GeV, SM couplings	vbfnlo	138.7 fb	4 500 000
WBF: $H \to \tau^+\tau^- \to lh + 3\nu$ $m_{\mathrm{H}} = 120$ GeV, CPE couplings	vbfnlo	–	1 500 000
WBF: $H \to \tau^+\tau^- \to lh + 3\nu$ $m_{\mathrm{H}} = 120$ GeV, CPO couplings	vbfnlo	–	1 500 000
WBF: $H \to W^+W^- \to ll\nu\nu$ $m_{\mathrm{H}} = 160$ GeV, SM couplings	vbfnlo	303.3 fb	4 500 000
WBF: $H \to W^+W^- \to ll\nu\nu$ $m_{\mathrm{H}} = 160$ GeV, CPE couplings	vbfnlo	–	1 500 000
WBF: $H \to W^+W^- \to ll\nu\nu$ $m_{\mathrm{H}} = 160$ GeV, CPO couplings	vbfnlo	–	1 500 000
gg fusion: $H \to \tau^+\tau^- \to ll + 4\nu$ $m_{\mathrm{H}} = 120$ GeV	Pythia	170.1 fb	300 000
gg fusion: $H \to \tau^+\tau^- \to lh + 3\nu$ $m_{\mathrm{H}} = 120$ GeV	Pythia	313.2 fb	900 000
gg fusion: $H \to W^+W^- \to ll\nu\nu$ $m_{\mathrm{H}} = 160$ GeV	Pythia	991.2 fb	1 200 000
$t\bar{t}$, W decays leptonic	Pythia	51.66 pb	65 000 000
Wt, one lepton filter (see text)	TopReX	26.66 pb	34 473 508
$WWjj$(EW), W decays leptonic	MadEvent	95.4 ± 1.1 fb	148 000
$WWjj$(QCD), W decays leptonic	MadEvent	1.392 ± 0.004 pb	1 911 562
Zjj(EW), Z decays leptonic	MadCUP	2.764 pb	3 152 807
Zjj(QCD), Z decays leptonic	MadCUP	26.12 pb	27 951 817

where the cut on the azimuthal angle between the tagging jets is omitted since this is the sensitive observable that is used later in the analysis. The changes are indicated in the list of cuts.

4.1 Motivation of the selection criteria

A typical feature of WBF events is the occurrence of two so-called tagging jets with a large pseudorapidity gap between them. They emerge from the two quarks that take part in the hard process and that are scattered preferentially in the forward direction. The tagging jets are required to have a minimum p_T and a minimum distance in η from each other. Since in contrast to QCD processes there is no colour flow between the quarks, there are usually no jets with a large p_T in the region between the tagging jets which is utilised by applying a veto on additional central jets.

In the channel $H \to W^+W^- \to ll\nu\nu$ the directions of the final state leptons are correlated. Since the Higgs boson is scalar the spins of the W bosons are aligned opposite to each other and the lepton and anti-lepton are emitted preferentially in the same direction. This is used by cutting on the angular variables of the leptons.

The fact that the transverse momentum of the tagging jets should be balanced by the transverse momentum of the Higgs boson is used in $H \to W^+W^- \to ll\nu\nu$ by cutting on the absolute value of the vector

$$p_T^{\text{tot}} = p_T^{l,1} + p_T^{l,2} + p_T^{\text{miss}} + p_T^{j,1} + p_T^{j,2} \qquad (16)$$

with the transverse momenta of the tagging jets $p_T^{j,1}$ and $p_T^{j,2}$, the transverse momenta of the leptons $p_T^{l,1}$ and $p_T^{l,2}$ and the missing transverse momentum p_T^{miss} which is at parton level given by the sum of the transverse momenta of the neutrinos. Since the absolute value of p_T^{tot} will only be small as long as there is no additional hard radiation this cut is correlated with the jet veto.

The contribution of the background processes $Z \to e^+e^-/\mu^+\mu^-$ in the channel $H \to W^+W^- \to ll\nu\nu$ can be suppressed by requiring the invariant mass of same flavour lepton pairs to lie outside a window around the Z boson mass. Additional suppression can be achieved by a cut on the transverse mass of the lepton–neutrino system

$$m_T \left(ll p_T^{\text{miss}}\right) = \sqrt{2P_T(ll)P_T^{\text{miss}}(1 - \cos\Delta\phi)} \qquad (17)$$

with the angle $\Delta\phi$ between the sum vector of the transverse momenta of the leptons $P_T(ll)$ and the missing transverse momentum vector.

In the $H \to \tau^+\tau^-$ channels the Higgs boson mass can be reconstructed from the transverse momenta of the decay products of the τ leptons and the missing transverse momentum. This reconstruction is described in Sect. 4.2. By selecting a window around the Higgs boson mass the $Z \to \tau^+\tau^-$ background can be suppressed.

Contributions from background processes with top quarks can be suppressed by requiring that the tagging jets have not been tagged as b-jets. For the tagging of b-jets

the default efficiency in ATHENA 10.0.1 of 50% is used. The probability for c-jets to be mistagged as b-jets is taken as $1/10.9$, the mistag probability for the remaining jets is $1/231$.

A lepton reconstruction efficiency of 90% is applied [20].

4.2 Reconstruction of the Higgs boson mass in $H \to \tau^+\tau^-$

The mass of the boson in the decay $H/Z \to \tau^+\tau^- \to ll + 4\nu$ can be reconstructed in the approximation that the transverse momenta of all decay products of a τ lepton are parallel to the transverse momentum of the τ lepton, the so-called collinear approximation. This approximation is justified as long as the absolute values of the transverse momenta of the τ leptons in the laboratory frame are sufficiently large. This is usually the case due to the large mass difference between the decaying boson and the τ lepton and the transverse momentum of the boson.

The mass reconstruction method can be applied both in the $H/Z \to \tau^+\tau^- \to ll + 4\nu$ and the $H/Z \to \tau^+\tau^- \to lh + 3\nu$ channels. The following refers to the case of the decay $\tau^+\tau^- \to ll + 4\nu$. For the case of the decay $\tau^+\tau^- \to lh + 3\nu$ one of the lepton momenta has to be replaced by the corresponding momentum of the object identified as a τ jet.

In the following all leptons are treated as massless. The fractions x_{τ_1} and x_{τ_2} of the τ lepton momenta that are carried by the observed leptons are defined as

$$x_{\tau_i} p_{\tau_i} = p_{l_i} . \qquad (18)$$

The fractions x_{τ_1} and x_{τ_2} can be calculated by using momentum conservation in the transverse plane:

$$p_{\tau_1}^T + p_{\tau_2}^T = \frac{p_{l_1}^T}{x_{\tau_1}} + \frac{p_{l_2}^T}{x_{\tau_2}} = p_{l_1}^T + p_{l_2}^T + p_{\text{miss}}^T . \qquad (19)$$

Solving for x_{τ_1} and x_{τ_2} gives:

$$x_{\tau_1} = \frac{p_{l_2}^x p_{l_1}^y - p_{l_1}^x p_{l_2}^y}{p_{l_2}^x p_{l_1}^y + p_{l_2}^x p_{\text{miss}}^y - p_{l_2}^y p_{l_1}^x - p_{l_2}^y p_{\text{miss}}^x} \qquad (20)$$

$$x_{\tau_2} = \frac{p_{l_1}^x p_{l_2}^y - p_{l_2}^x p_{l_1}^y}{p_{l_1}^x p_{l_2}^y + p_{l_1}^x p_{\text{miss}}^y - p_{l_1}^y p_{l_2}^x - p_{l_1}^y p_{\text{miss}}^x} . \qquad (21)$$

From this the mass of the boson is calculated as

$$m_{\tau\tau} = \sqrt{(p_{\tau_1} + p_{\tau_2})^2} = \sqrt{2p_{\mu\tau_1}p_{\tau_2}^\mu} = \frac{m_{ll}}{\sqrt{x_{\tau_1}x_{\tau_2}}} . \qquad (22)$$

### 4.3 Selection cuts for $H \to W^+W^- \to ll\nu\nu$

1. jet and lepton acceptance: Two observed candidates for the tagging jets are required. Tagging jet candidates are the jet with the largest p_T in the region $\eta < 0$ and the jet with the largest p_T in the region $\eta > 0$. In addition two observed leptons with $|\eta| < 2.5$ are required. One lepton must have $p_T > 20$ GeV and the other one $p_T > 15$ GeV.

2. b-jet veto: The tagging jet candidates must not have been tagged as b-jets.
3. tagging jet identification: One tagging jet candidate must have $p_T > 40$ GeV, the other one must have $p_T > 20$ GeV. There must be a gap in pseudorapidity of at least $\Delta\eta > 3.8$ between the tagging jet candidates. The leptons must have pseudorapidities between those of the tagging jet candidates: $\eta_{tag}^{min} < \eta_{l_{1,2}} < \eta_{tag}^{max}$.
4. lepton cuts: For the decay leptons $\Delta\phi_{ll} < 1.05$, $\Delta R_{ll} < 1.8$, $\cos\theta_{ll} > 0.2$, $m_{ll} < 85$ GeV and $p_T(l) < 120$ GeV are required, with the azimuthal angle around the beam axis between the lepton momenta $\Delta\phi_{ll}$, the distance in the η-ϕ-plane between the lepton momenta ΔR_{ll}, the cosine of the polar angle with respect to the beam axis between the lepton momenta $\cos\theta_{ll}$, the invariant mass of the lepton pair m_{ll} and the transverse momentum of each lepton $p_T(l)$.
5. $Z \to \tau^+\tau^-$ suppression: Events with $x_{\tau_1} > 0$ and $x_{\tau_2} > 0$ and $|m_{\tau\tau} - m_Z| < 25$ GeV are discarded.
6. invariant mass of the tagging jet pair: $m_{jj} > 550$ GeV.
7. momentum balance: $|p_T^{tot}| < 30$ GeV.
8. central jet veto: No jets with $p_T > 20$ GeV that are not tagging jets are allowed in the region $|\eta| < 3.2$.
9. $Z \to e^+e^-/\mu^+\mu^-$ suppression: Events with same flavour lepton pairs are required to have $m_{ll} < 75$ GeV and $p_T^{miss} > 30$ GeV.
10. $m_T\left(llp_T^{miss}\right)$ cut: $m_T\left(llp_T^{miss}\right) > 30$ GeV.

The results of the cut analysis in this channel are listed in Table 6. The distribution in the last cut variable is shown in Fig. 3. Due to the choice of cuts at the generator level the Zjj event samples could not be used as background samples in this channel. However, it was shown in [1] that the contribution from Zjj is small after all cuts. The expected signal significance, using Poisson statistics and treating the gluon–gluon–fusion process as a part of the signal, is 24 for an integrated luminosity of 30 fb^{-1} and a Higgs boson mass of 160 GeV.

4.4 Selection cuts for $H \to \tau^+\tau^- \to ll + 4\nu$

1. jet and lepton acceptance: Two observed candidates for the tagging jets are required. The candidates are selected as in the channel $H \to W^+W^- \to ll\nu\nu$. In addition, cuts based on the current trigger conditions for leptons (one- or two-lepton trigger) have to be satisfied.
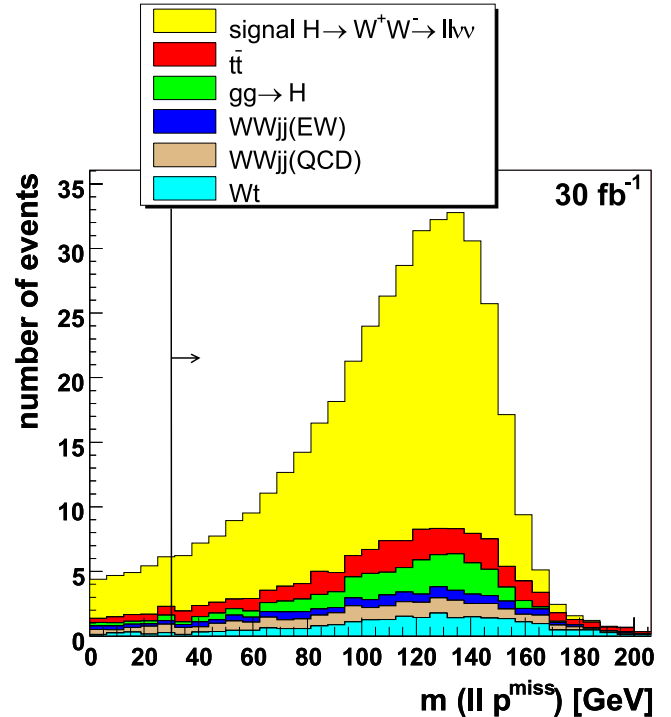
Fig. 3. Distribution of the expected number of events in the last cut variable $m_T(llp_T^{miss})$ in the channel $H \to W^+W^- \to ll\nu\nu$ for an integrated luminosity of 30 fb^{-1}. All cuts except the last one have been applied. All generated Monte Carlo events have been used and the distributions have been scaled to the respective expected number of events

These cuts require *either* one isolated electron with $p_T > 25$ GeV *or* a muon with $p_T > 20$ GeV *or* two isolated electrons with $p_T > 15$ GeV *or* two muons with $p_T > 10$ GeV *or* an isolated electron with $p_T > 15$ GeV together with a muon with $p_T > 10$ GeV. At least two observed leptons with $|\eta| < 2.5$ are required. The two leptons with the largest p_T are selected.
2. b-jet veto: The tagging jet candidates must not have been tagged as b-jets.
3. tagging jet identification: One tagging jet candidate must have $p_T > 50$ GeV, the other one must have $p_T > 30$ GeV. There must be a gap in pseudorapidity of $\Delta\eta > 4.4$ between the tagging jet candidates. The leptons must have pseudorapidities between those of the tag-

Table 6. Results of the event selection for the channel $H \to W^+W^- \to ll\nu\nu$. Statistical errors are given where known and non-negligible

|	$\sigma \cdot$BR before cuts	$\sigma \cdot$BR after cuts	events expected for 30 fb^{-1} after cuts
signal	303.3 fb	9.46 ± 0.02 fb	284 ± 1
gg fusion	991.2 fb	0.96 ± 0.03 fb	29 ± 1
$t\bar{t}$	51.66 pb	1.23 ± 0.03 fb	37 ± 1
Wt	26.66 pb	0.77 ± 0.02 fb	23 ± 1
$WWjj$(EW)	95.4 ± 1.1 fb	0.43 ± 0.02 fb	13 ± 1
$WWjj$(QCD)	1.392 ± 0.004 pb	0.69 ± 0.02 fb	21 ± 1

ging jet candidates. There must be a gap in pseudora-
pidity of $\Delta\eta > 0.7$ between a tagging jet candidate and
a lepton: $\eta_{\mathrm{tag}}^{\min} + 0.7 < \eta_{1,2} < \eta_{\mathrm{tag}}^{\max} - 0.7$. The require-
ment of a gap in η between the momenta of the leptons
and the tagging jets was added with respect to [1].
4. missing transverse momentum: $p_{\mathrm{T}}^{\mathrm{miss}} > 50$ GeV.
5. invariant mass of the tagging jet pair: $m_{jj} > 700$ GeV.
6. central jet veto: No jets with $p_{\mathrm{T}} > 20$ GeV that are not
   tagging jets are allowed in the region $|\eta| < 3.2$.
7. distance between lepton momenta: $\Delta R_{ll} < 2.4$ is re-
   quired. This cut was tightened with respect to [13]
   where $\Delta R_{ll} < 2.6$ was required.
8. reconstruction of τ lepton momenta: $x_{\tau_1} > 0$ and $x_{\tau_2} >$
   0 and $x_{\tau_1}^2 + x_{\tau_2}^2 < 1$ are required.
9. Higgs boson mass window: $110\,\mathrm{GeV} < m_{\tau\tau} < 135\,\mathrm{GeV}$.

The results of the cut analysis in this channel are listed in
Table 7. The distribution in the last cut variable is shown
in Fig. 4. The expected signal significance, using Poisson
statistics and treating the gluon–gluon–fusion process as
a part of the signal, is 4.7 for an integrated luminosity of
$30\,\mathrm{fb}^{-1}$ and a Higgs boson mass of 120 GeV.

4.5 Selection cuts for $H \to \tau^+\tau^- \to lh + 3\nu$

1. jet and lepton acceptance: Two observed candidates
   for the tagging jets are required. The candidates are
   selected as in the channel $H \to W^+W^- \to ll\nu\nu$. In
   addition, one observed isolated electron with $|\eta| < 2.5$
   and $p_{\mathrm{T}} > 25$ GeV or one observed muon with $|\eta| < 2.5$
   and $p_{\mathrm{T}} > 20$ GeV is required (single-lepton trigger
   requirement).
2. b-jet veto: The tagging jet candidates must not have
   been tagged as b-jets.
3. hadronic τ lepton decay: One jet labelled as a τ-jet
   as described in [11] is required. The jet must have
   $p_{\mathrm{T}} > 40$ GeV.
4. tagging jet identification: One tagging jet candidate
   must have $p_{\mathrm{T}} > 40$ GeV, the other one must have $p_{\mathrm{T}} >$
   20 GeV. There must be a gap in pseudorapidity of $\Delta\eta >$
   4.4 between the tagging jet candidates. The leptons
   must have pseudorapidities between those of the tag-
   ging jet candidates: $\eta_{\mathrm{tag}}^{\min} < \eta_{l,h} < \eta_{\mathrm{tag}}^{\max}$.
5. reconstruction of τ lepton momenta: $0 < x_{\tau_l} < 0.75$ and
   $0 < x_{\tau_h} < 1$ are required.
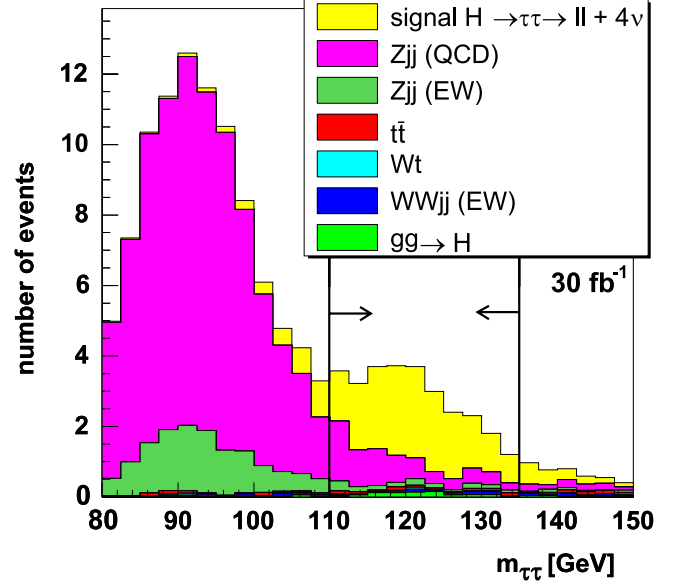
Fig. 4. Distribution of the expected number of events in the
last cut variable, the invariant mass of the τ lepton pair, in the
channel $H \to \tau^+\tau^- \to ll + 4\nu$ for an integrated luminosity of
$30\,\mathrm{fb}^{-1}$. All cuts except the last one have been applied. All gen-
erated Monte Carlo events have been used and the distributions
have been scaled to the respective expected number of events

6. transverse mass:
   $m_{\mathrm{T}}\left(lp_{\mathrm{T}}^{\mathrm{miss}}\right) = \sqrt{2p_{\mathrm{T}}(l)p_{\mathrm{T}}^{\mathrm{miss}}(1 - \cos\Delta\phi)} < 30$ GeV.
7. missing transverse momentum: $p_{\mathrm{T}}^{\mathrm{miss}} > 30$ GeV.
8. invariant mass of the tagging jet pair: $m_{jj} > 700$ GeV.
9. central jet veto: No jets with $p_{\mathrm{T}} > 20$ GeV are allowed in
   the pseudorapidity region between the tagging jets.
10. Higgs boson mass window: $110\,\mathrm{GeV} < m_{\tau\tau} < 135\,\mathrm{GeV}$.

The results of the cut analysis in this channel are listed in
Table 8. The distribution in the last cut variable is shown
in Fig. 5. The analysis in this channel requires the iden-
tification of the decay products coming from hadronic τ
lepton decays. Since the identification of hadronic τ lep-
ton decays in ATLFAST-B does not give correct results
in ATHENA 10.0.1 [21] the identification efficiency is ap-
plied by discarding 50% of all events. It is assumed that
the main background in this channel comes from hadronic

Table 7. Results of the event selection for the channel $H \to \tau^+\tau^- \to ll + 4\nu$. Statistical errors
are given where known and non-negligible

	$\sigma\cdot$BR before cuts	$\sigma\cdot$BR after cuts	events expected for $30\,\mathrm{fb}^{-1}$ after cuts
signal	37.67 fb	0.61 fb	18
gg fusion	170.1 fb	0.03 fb	1
$t\bar{t}$	51.66 pb	0.02 fb	1
Wt	26.67 pb	0.01 fb	0
$WWjj$(EW)	95.4 ± 1.1 fb	0.02 fb	1
Zjj(EW)	2.76 pb	0.05 ± 0.01 fb	2
Zjj(QCD)	26.12 pb	0.23 ± 0.01 fb	7

Table 8. Results of the event selection for the channel $H \to \tau^+\tau^- \to lh + 3\nu$. Statistical errors are given where known and non-negligible

|	$\sigma \cdot \mathrm{BR}$ before cuts	$\sigma \cdot \mathrm{BR}$ after cuts	events expected for 30 fb^{-1} after cuts
signal	138.7 fb	0.46 fb	14
gg fusion	313.2 fb	0.02 fb	1
Zjj(EW)	2.76 pb	0.03 ± 0.01 fb	1
Zjj(QCD)	26.12 pb	0.18 ± 0.01 fb	5
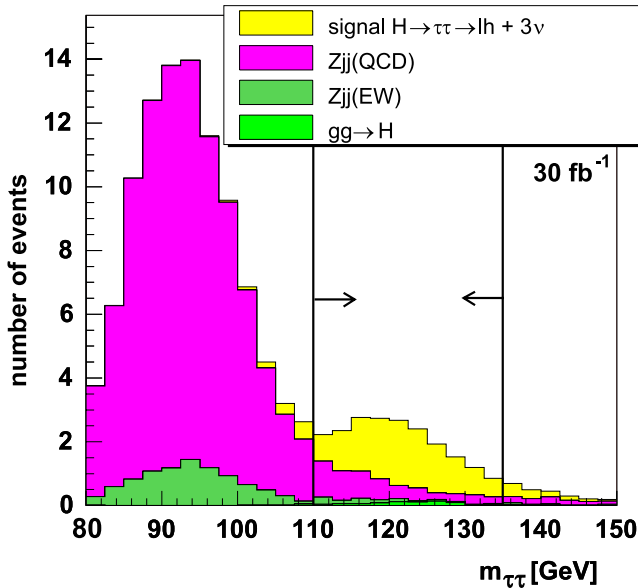
Fig. 5. Distribution of the expected number of events in the last cut variable, the invariant mass of the τ lepton pair, in the channel $H \to \tau^+\tau^- \to lh + 3\nu$ for an integrated luminosity of 30 fb^{-1}. All cuts except the last one have been applied. All generated Monte Carlo events have been used and the distributions have been scaled to the respective expected number of events

τ lepton decays in the process $Z \to \tau^+\tau^-$. The possibility of misidentified hadronic τ decay products is not taken into account. Hence, only the Zjj and gluon–gluon–fusion background samples are used for the analysis in this channel. Contributions from other background processes were evaluated in [1] and shown to be small after all cuts. Since the energy calibration in ATLFAST-B does not give the correct results for hadronic τ decay products [21] the uncalibrated energy is used for the jets labelled as τ-jets. The expected signal significance, using Poisson statistics and treating the gluon–gluon–fusion process as a part of the signal, is 4.3 for an integrated luminosity of 30 fb^{-1} and a Higgs boson mass of 120 GeV.

4.6 Comparison of vbfnlo with Pythia

The event samples generated with vbfnlo with standard model couplings are compared to WBF event samples generated with Pythia to check the consistency between the two generators. It was already pointed out in Sect. 3.1

that the parameter PARP(71), which controls the cut-off scale for the final state parton shower, has to be changed from its default value in ATHENA 10.0.1 of 4 to 1 when vbfnlo is used as an external event generator to achieve the same parton shower behaviour as when Pythia is used to generate the events. A variable that is particularly sensitive to the value of PARP(71) is $|p_{\mathrm{T}}^{\mathrm{tot}}|$. The distribution of $|p_{\mathrm{T}}^{\mathrm{tot}}|$ is shown in Fig. 6 for events generated with vbfnlo for two different values of PARP(71) and for events generated with Pythia. One can see that the distributions from vbfnlo and Pythia agree for $PARP(71) = 1$ while they differ significantly for $PARP(71) = 4$. The efficiency of the cut on $|p_{\mathrm{T}}^{\mathrm{tot}}|$ increases by about 15% relative to the value for $PARP(71) = 4$ when PARP(71) is changed from 4 to 1. The efficiency of the whole event selection increases by about 30%. There is no a priori reason to prefer one value of PARP(71) over the other but for consistency with analyses that use Pythia for the event generation the value of PARP(71) is set to 1 in this study. Figures 7 and 8 show distributions of some cut variables for the channel $H \to W^+W^- \to ll\nu\nu$ from the final vbfnlo event sample with standard model couplings and from a control sample generated with
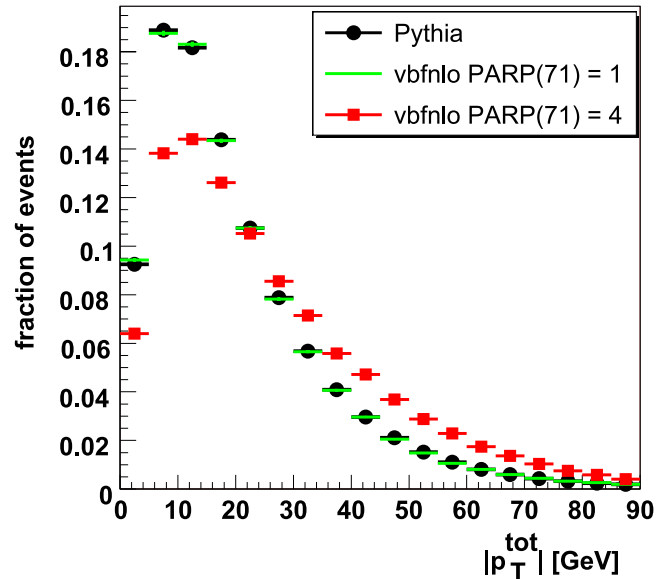
Fig. 6. Distribution of $|p_{\mathrm{T}}^{\mathrm{tot}}|$ in the channel $H \to W^+W^- \to ll\nu\nu$ after detector simulation and before cuts from events generated with Pythia and from events generated with vbfnlo for two different values of the parameter PARP(71) (see text)
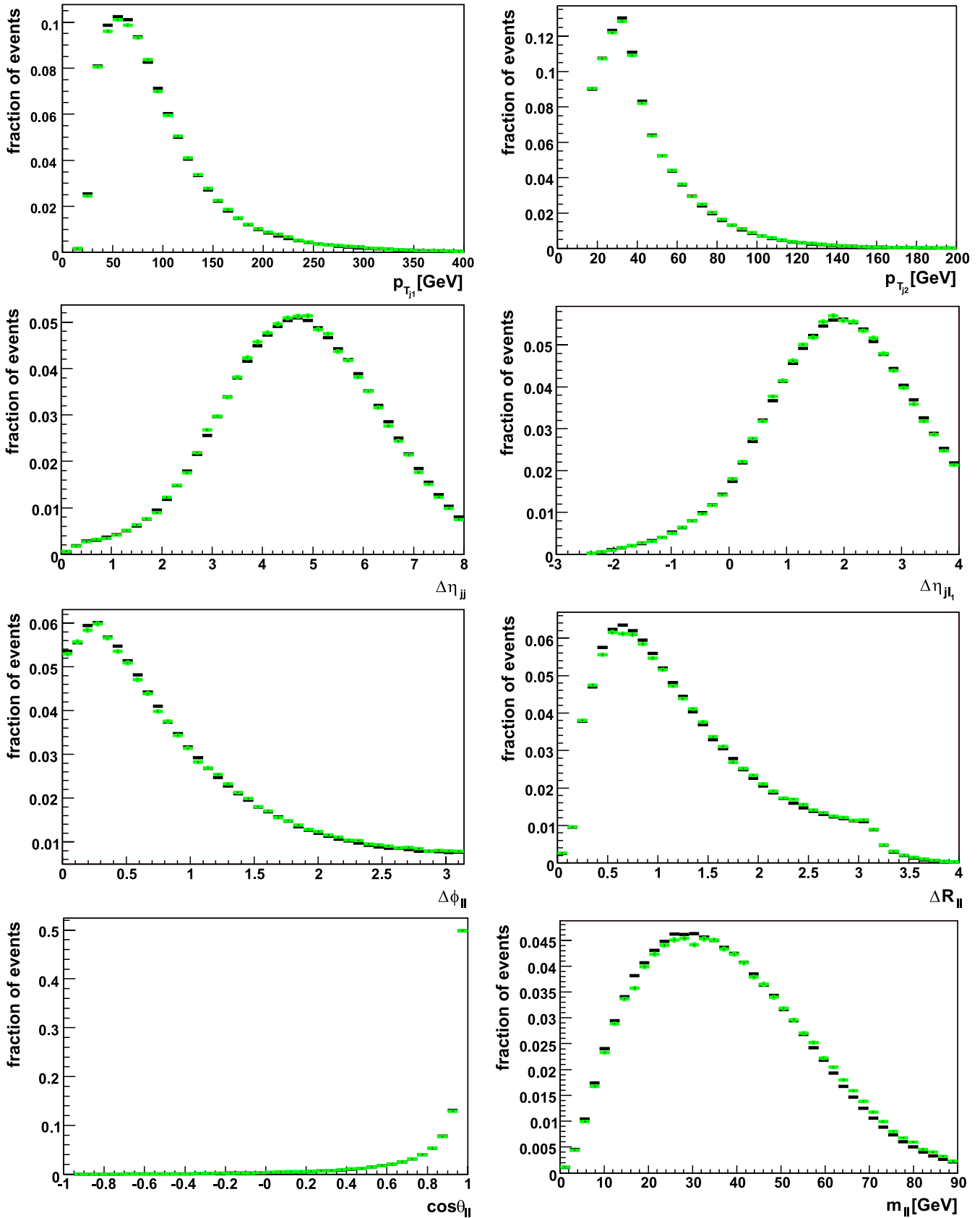
Fig. 7. Distributions of some of the cut variables for the channel $H \to W^+ W^- \to ll\nu\nu$ after the detector simulation and before cuts. The distributions from events generated with vbfnlo are drawn in *black*, the distributions from events generated with Pythia are drawn in *green* (*light grey*)
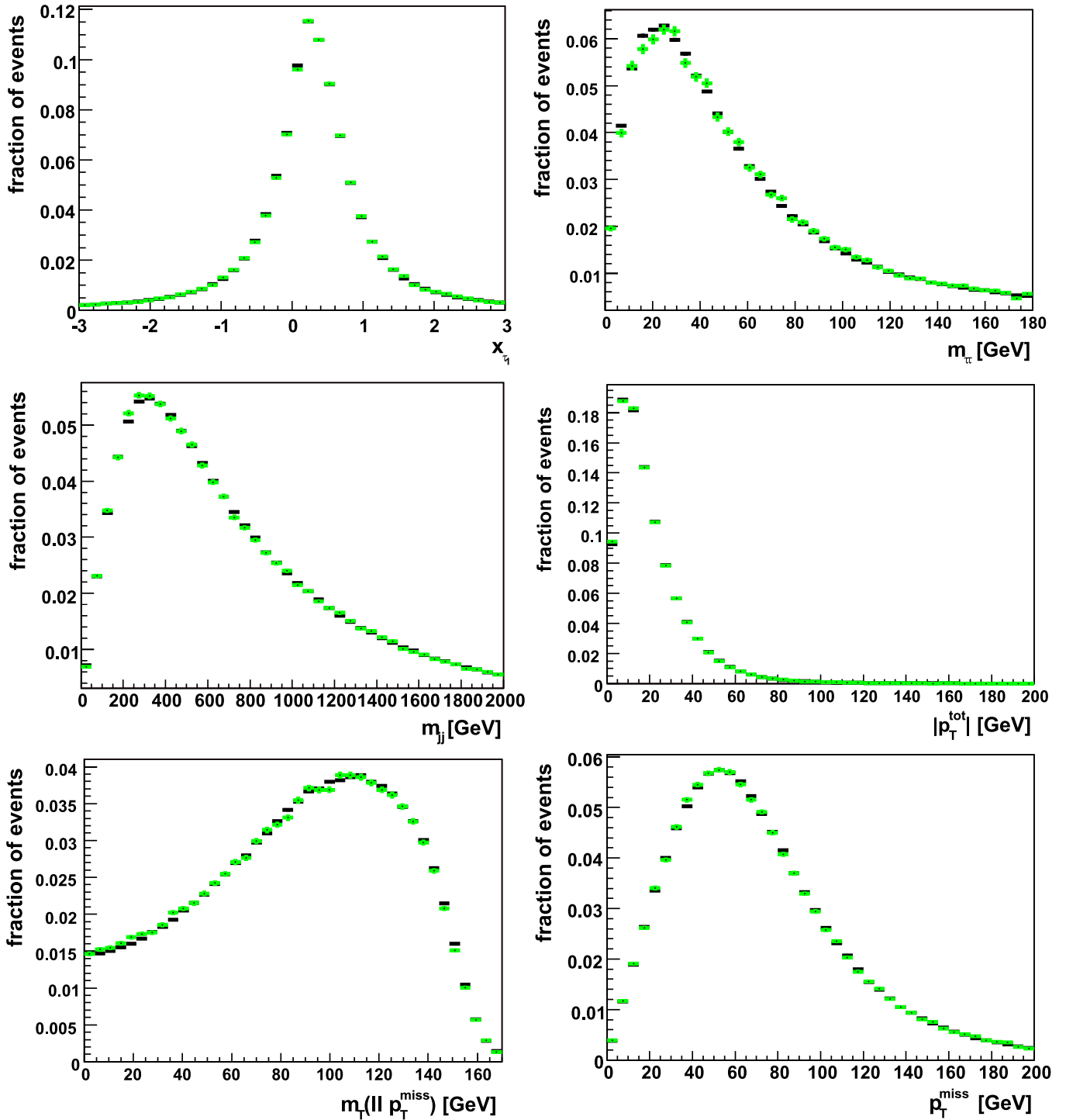
Fig. 8. Distributions of some of the cut variables for the channel $H \to W^+W^- \to ll\nu\nu$ after the detector simulation and before cuts. The distributions from events generated with vbfnlo are drawn in *black*, the distributions from events generated with Pythia are drawn in *green* (*light grey*)

Pythia. One can see that the remaining differences are small.

The event selection in the $H \to \tau^+\tau^-$ channels is less sensitive to the value of PARP(71). With $PARP(71) = 1$ the differences between vbfnlo and Pythia in these channels are small as in the case of $H \to W^+W^-$.

5 Determination of the dominant coupling term

After the discovery of a new scalar particle at the LHC a question of interest is by which of the 3 coupling terms presented in Sect. 2 the coupling to weak bosons is de-

scribed. By distinguishing between the CP even and the CP odd coupling terms one obtains information about the CP quantum number of the particle and by distinguishing between the standard model coupling term and the anomalous coupling terms one can test whether the coupling exists at leading order or is mediated by particle loops. In this section a hypothesis test is described in which the shape of the distribution of the azimuthal angles between the tagging jets $\Delta\phi_{jj}$ is used, as suggested in [2], to distinguish between the different couplings. The method is applied to the case of a standard model Higgs boson for which the prospects for the experimental exclusion of the anomalous couplings are investigated.

5.1 Implementation of the hypothesis test

A χ^2 test is performed in the distribution of the variable $\Delta\phi_{jj}$ after the event selection has been applied. Figure 9 shows distributions of $\Delta\phi_{jj}$ for signal events with the three different couplings and for all three channels. One can see that the distributions are similar for the three different channels, the main difference being that large values of

$\Delta\phi_{jj}$ are somewhat suppressed by the selection cuts in the $H \to \tau^+\tau^-$ channels. The distributions for the standard model case are fairly flat. The distributions for a CP odd anomalous coupling have a maximum at $\pi/2$ and they are close to 0 for collinear p_T of the tagging jets while the distributions for a CP even anomalous coupling show the opposite features.

From each signal and background event sample a reference distribution is calculated using the full statistics. The normalisation of the signal relative to the background in the standard model case follows from the standard model cross sections. For the case of anomalous couplings the normalisation is chosen such that the ratio of the number of signal events to the number of background events after cuts is the same as in the case of standard model couplings. With this choice of normalisation, the question that is investigated is whether for a scalar particle that has the expected experimental signature of a standard model Higgs boson the dominant coupling term can be determined. A prediction of the total cross section for the signal process for purely anomalous couplings is not necessary because only the shape of the signal distribution is used in the test. In an analysis with experimental data a differ-
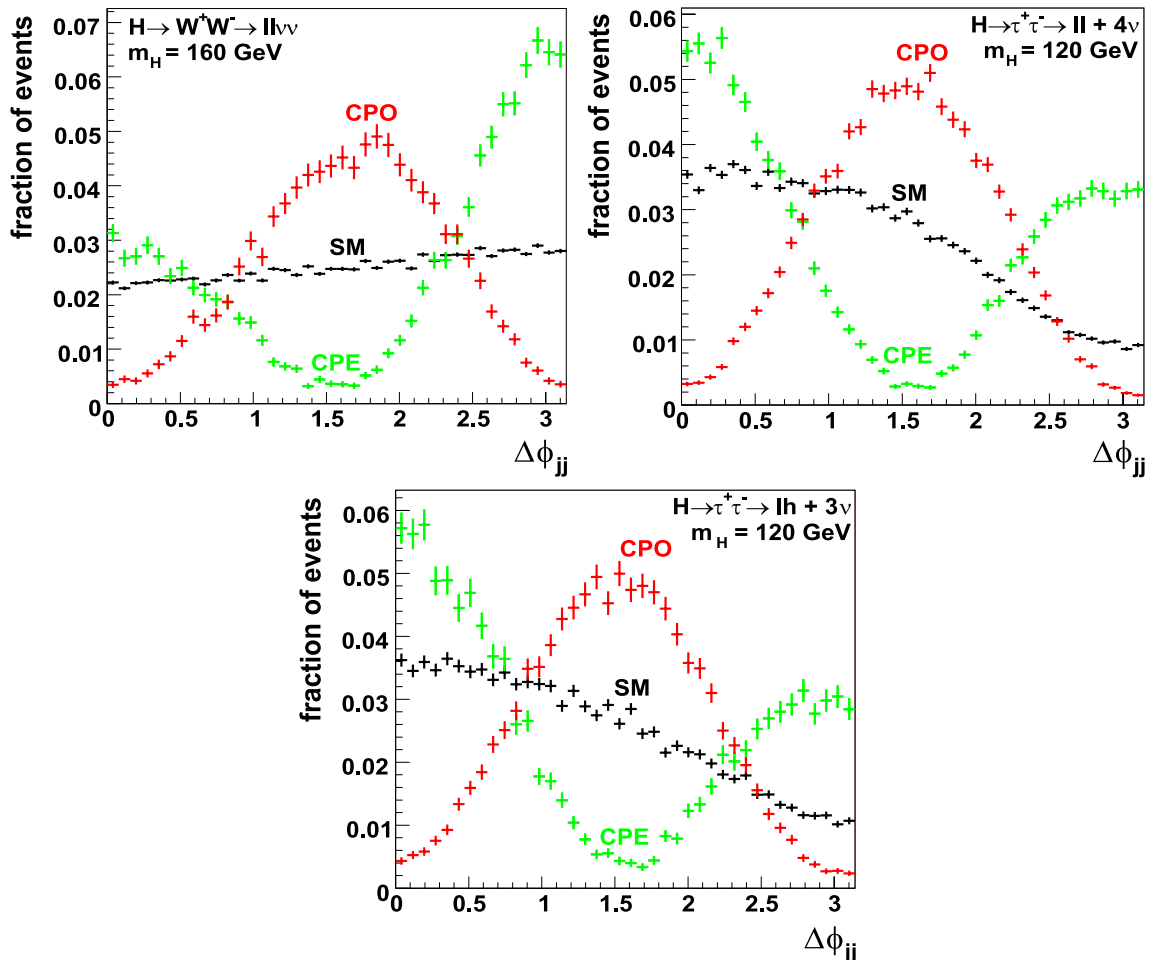
Fig. 9. Distributions of the variable $\Delta\phi_{jj}$ with high statistics for signal events after all cuts have been applied. Distributions are shown for each of the three different couplings and each of the channels studied

ent relative normalisation of signal and background may be preferred. This may be a value determined from experiment or from the predictions of a different model containing a scalar particle.

The hypothesis test is performed on Monte Carlo pseudo-data samples containing signal events with standard model couplings and standard model background events corresponding to the expected amount of data after the first few years of data taking at the LHC at low luminosity. For the channel $H \to W^+W^- \to ll\nu\nu$ pseudo-data samples containing both standard model Higgs boson and background contributions corresponding to integrated luminosities of $10\,\mathrm{fb}^{-1}$ and $30\,\mathrm{fb}^{-1}$ are formed. For the $H \to \tau^+\tau^-$ channels pseudo-data samples are formed only for $30\,\mathrm{fb}^{-1}$. The pseudo-data samples are built from subsamples of the complete Monte Carlo samples from which the reference distributions are also calculated. Since the complete samples contain at least by a factor of 30 more events than the pseudo-data samples the pseudo-data samples are assumed to be sufficiently statistically independent from the complete samples. Furthermore, the number of events in the complete samples is assumed to be sufficiently large with respect to the number of events in the pseudo-data

samples for the statistical errors on the reference distributions to be negligible.

The χ^2 is calculated for the number of bin entries n_i of a histogram of $\Delta\phi_{jj}$ for a pseudo-data sample and the number of bin entries of a reference histogram ν_i as

$$\chi^2 = \sum_i \frac{\left(n_i - \frac{\nu_i n}{\nu}\right)^2}{\frac{\nu_i n}{\nu}} \tag{23}$$

with $n = \sum n_i$ and $\nu = \sum \nu_i$.

5.2 Application to a few individual pseudo-data samples

Some features of the test can be illustrated with exemplary results for individual pseudo-data samples. Figure 10 shows the distributions of $\Delta\phi_{jj}$ for one pseudo-data sample per channel together with the reference distributions for anomalous couplings which are normalised to the number of events in the pseudo-data distribution. One can see that the number of events in the $H \to \tau^+\tau^-$ channels is
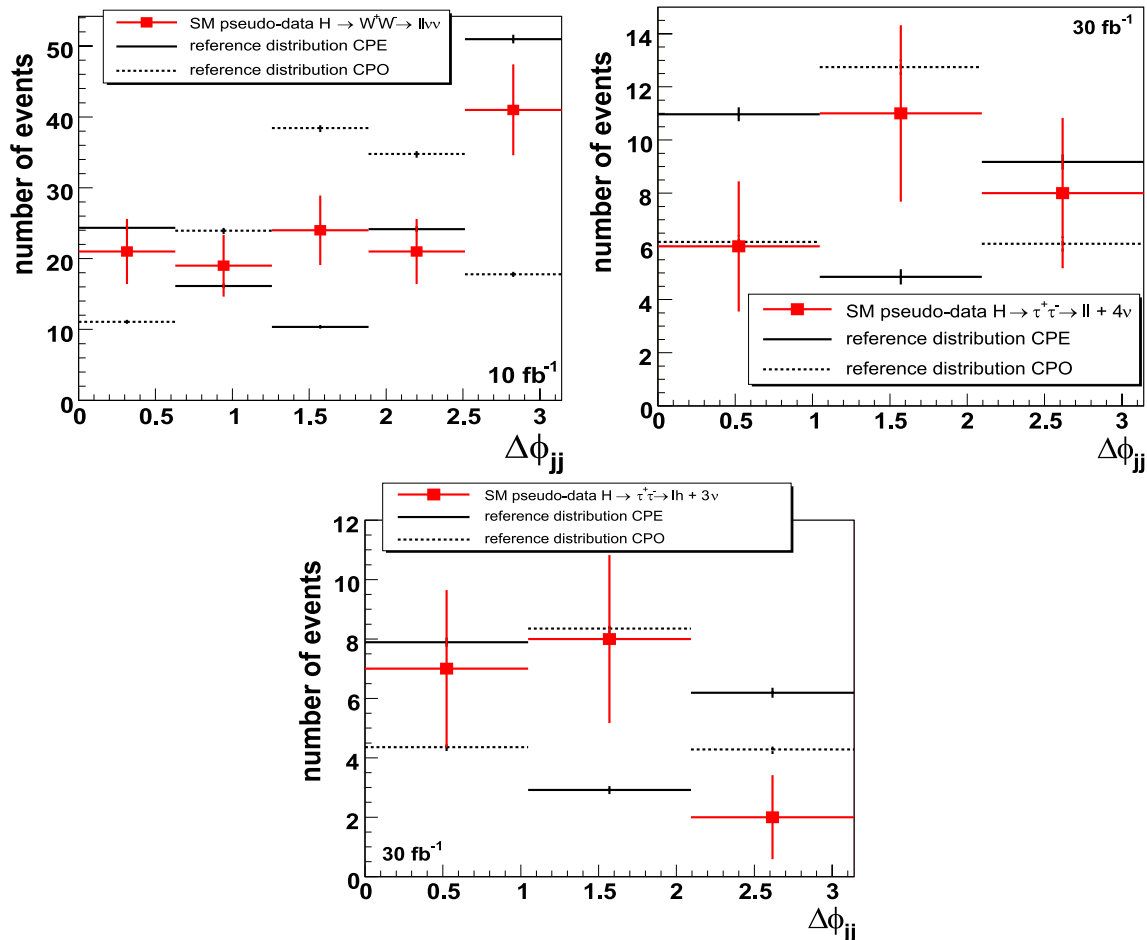
Fig. 10. Distributions of $\Delta\phi_{jj}$ for one exemplary pseudo-data sample per channel. The reference distributions for the case of anomalous couplings shown are normalised to the number of entries of the pseudo-data histograms. Both pseudo-data and reference distributions include contributions from background processes

Table 9. Results of the χ^2 test for one standard model pseudo-data sample per channel and integrated luminosity studied for the hypotheses of purely CP even and purely CP odd anomalous couplings (CPO). The upper table shows the results for samples in which background contributions are included. The lower table gives the values for the same signal events without background contributions for comparison. For the $H \to \tau^+\tau^-$ case results are given for the channel $H \to \tau^+\tau^- \to ll + 4\nu$ and for both $H \to \tau^+\tau^-$ channels combined

background included: hypothesis		$H \to W^+W^- \to ll\nu\nu$	$H \to \tau^+\tau^- \to ll + 4\nu$	$H \to \tau^+\tau^-$ combined
$10\,\mathrm{fb}^{-1}$	CPE	$2.8 \times 10^{-4} \,\hat{=}\, 3.6\sigma$		
	CPO	$2.1 \times 10^{-10} \,\hat{=}\, 6.4\sigma$		
$30\,\mathrm{fb}^{-1}$	CPE	$< 10^{-15} \,\hat{=}\, > 7.7\sigma$	$6.2 \times 10^{-3} \,\hat{=}\, 2.7\sigma$	$2.0 \times 10^{-4} \,\hat{=}\, 3.7\sigma$
	CPO	$< 10^{-15} \,\hat{=}\, > 7.7\sigma$	$6.6 \times 10^{-1} \,\hat{=}\, 0.44\sigma$	$4.5 \times 10^{-1} \,\hat{=}\, 0.76\sigma$
background not included, for comparison: hypothesis		$H \to W^+W^- \to ll\nu\nu$	$H \to \tau^+\tau^- \to ll + 4\nu$	$H \to \tau^+\tau^-$ combined
$10\,\mathrm{fb}^{-1}$	CPE	$3.3 \times 10^{-14} \,\hat{=}\, 7.6\sigma$		
	CPO	$< 10^{-15} \,\hat{=}\, > 7.7\sigma$		
$30\,\mathrm{fb}^{-1}$	CPE	$< 10^{-15} \,\hat{=}\, > 7.7\sigma$	$2.2 \times 10^{-8} \,\hat{=}\, 5.6\sigma$	$4.1 \times 10^{-9} \,\hat{=}\, 5.9\sigma$
	CPO	$< 10^{-15} \,\hat{=}\, > 7.7\sigma$	$7.2 \times 10^{-1} \,\hat{=}\, 0.36\sigma$	$3.5 \times 10^{-1} \,\hat{=}\, 0.93\sigma$

quite small even for $30\,\mathrm{fb}^{-1}$. Hence, the test is performed in 3 bins. The results from the channels $H \to \tau^+\tau^- \to ll + 4\nu$ and $H \to \tau^+\tau^- \to lh + 3\nu$ are combined by adding the χ^2 values for the histograms of both channels. In the channel $H \to W^+W^- \to ll\nu\nu$ the test is performed in 5 bins for $10\,\mathrm{fb}^{-1}$ and in 10 bins for $30\,\mathrm{fb}^{-1}$.

The results for the χ^2 probability are shown in Table 9. For each χ^2 probability the corresponding deviation from the mean of a Gaussian is calculated with a χ^2 probability of 5.73×10^{-7} corresponding to a deviation of 5σ. Results are given for the samples containing signal and background events and for comparison for the same signal events without background contributions. One can see that the χ^2 probabilities differ by several orders of magnitude and that the corresponding deviation from the mean of a Gaussian changes by a factor of up to 2 when background events are neglected. For the tested samples a clear exclusion of the anomalous couplings is possible in the channel $H \to W^+W^- \to ll\nu\nu$ at $30\,\mathrm{fb}^{-1}$ with good evidence already at $10\,\mathrm{fb}^{-1}$. For the tested samples in the $H \to \tau^+\tau^-$ channels only the hypothesis of a CP even anomalous coupling can be excluded at a high confidence level. The results for CP even and CP odd anomalous couplings appear to be correlated. If the limit on one of the couplings is strong the pseudo-data distribution will typically look similar to the reference distribution of the other anomalous coupling. This can be seen for the examples in Fig. 10 in which the pseudo-data distributions for the channel $H \to W^+W^- \to ll\nu\nu$ look more similar to the CP even anomalous reference distribution while the pseudo-data distributions for the $H \to \tau^+\tau^-$ channels both look more similar to the CP odd anomalous reference distribution.

5.3 Application to many pseudo-data samples

The χ^2 test is repeated for many pseudo-data samples to obtain average values and distributions of the χ^2 probabilities.

As a first step disjoint subsamples are taken from the complete Monte Carlo samples. For an integrated luminosity of $10\,\mathrm{fb}^{-1}$ the size of the Monte Carlo samples permits forming 149 subsamples in this way and for an integrated luminosity of $30\,\mathrm{fb}^{-1}$ 49 subsamples can be formed in the channel $H \to W^+W^- \to ll\nu\nu$ and 44 subsamples can be formed in the $H \to \tau^+\tau^-$ channels. To increase the number of samples further subsamples are formed by resampling [22]. This method consists in taking events randomly from the complete Monte Carlo samples until the desired number is reached. An event that has been chosen is not marked and can be chosen again, even for the same pseudo-data sample. 10 000 pseudo-data samples per channel are formed in this way. Effects of correlations between the samples due to events appearing in multiple samples and sometimes multiple times in the same sample are not investigated in this study.

The method is verified by calculating distributions of the χ^2 probabilities with the reference distributions for standard model couplings. Since the hypothesis tested in this case is true the distributions of the χ^2 probabilities must be flat within statistical fluctuations. The distributions are shown in Fig. 11 and one can see that they agree with the expectation.

Distributions of the χ^2 probabilities for the hypotheses of CP even and CP odd anomalous couplings are shown in Figs. 12 and 13. From the distributions the probability of a pseudo-data sample to have a χ^2 probability below a given threshold can be calculated. This can be interpreted as an estimate of the probability to obtain a χ^2 probability at the threshold value or below from a standard model event sample of the given integrated luminosity at the ATLAS experiment. These probabilities are given in Table 10 for the pseudo-data samples from resampling and for threshold values of the χ^2 probability of 5% and a value corresponding to 5σ. In addition the median χ^2 probability and the corresponding deviation from the mean of a Gaussian distribution in standard deviations are given for the channels in which more than half of the pseudo-data sam-
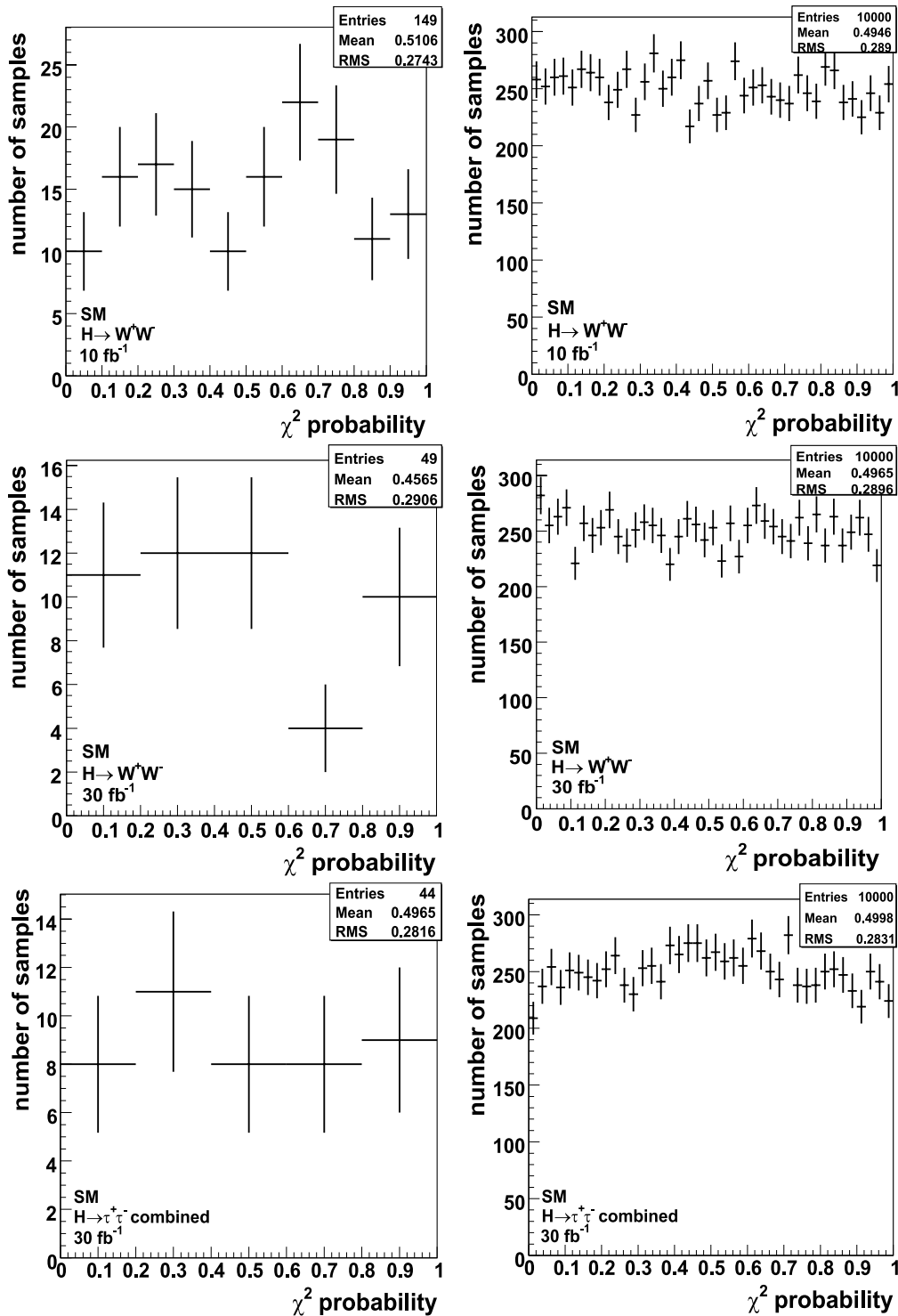
Fig. 11. Control distributions of the χ^2 probabilities for the standard model hypothesis. Distributions for disjoint subsamples are shown on the *left* and distributions for pseudo-data samples from resampling are shown on the *right*

ples have a χ^2 probability above 10^{-15} which is the limit of the numerical precision of the calculation.

5.3.1 Results of the hypothesis test

According to the results in Table 10 it appears to be possible to exclude *purely anomalous* CP even and *purely anomalous* CP odd couplings for a standard model Higgs boson at $m_H = 160\,\text{GeV}$ in the channel $H \to W^+W^- \to ll\nu\nu$ already from $10\,\text{fb}^{-1}$ of low luminosity data at a confidence level corresponding to approximately 5σ. For a standard model Higgs boson at $m_H = 120\,\text{GeV}$ in the $H \to \tau^+\tau^-$ channels the expected limits for the exclusion are weaker. However, on average an exclusion with a confidence level corresponding to 2σ or more is expected for an integrated luminosity of $30\,\text{fb}^{-1}$.
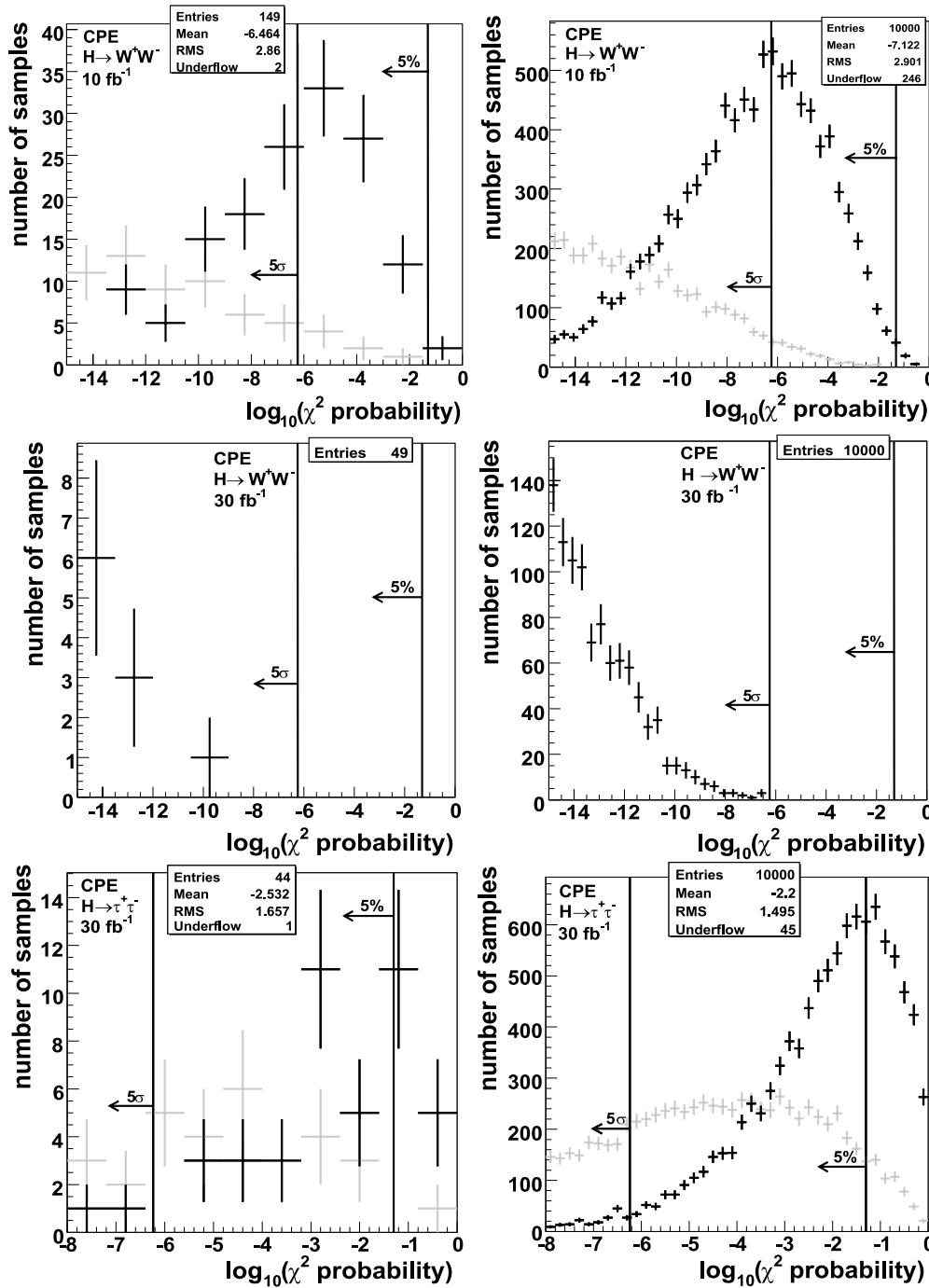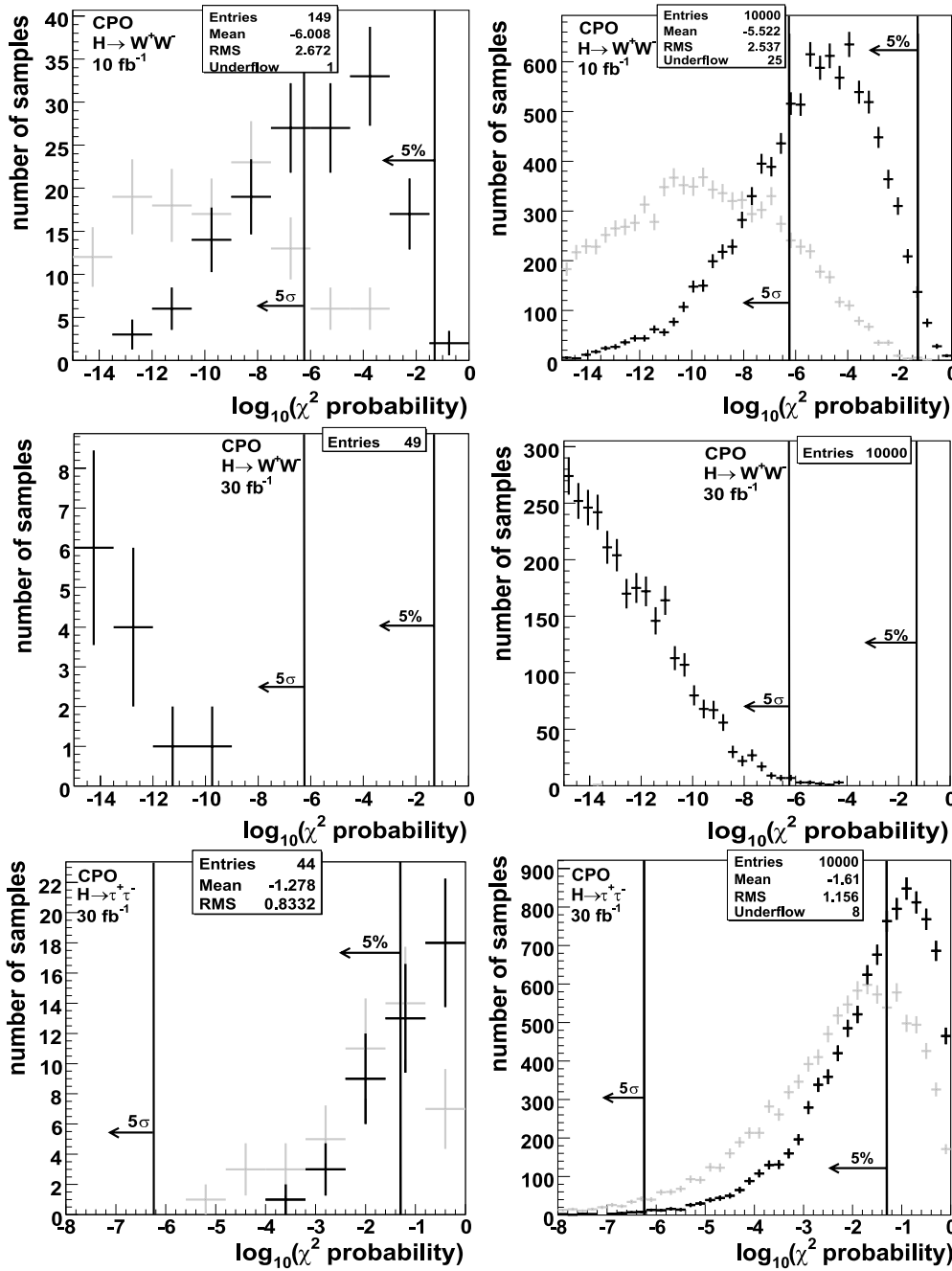
Fig. 12. Distributions of χ^2 probabilities for the hypothesis of a purely anomalous CP even coupling. Distributions for disjoint subsamples are shown on the *left* and distributions for pseudo-data samples from resampling are shown on the *right*. For comparison distributions in which background contributions have been neglected are shown in *grey*. The distributions are only shown down to a value of 10^{-15} which is the limit of the numerical precision of the calculation

5.4 Effects of uncertainties on the number of background events

The total number of background events in a data sample from the ATLAS detector is estimated in [1] to be measurable with an uncertainty of ±10%. The effect on the χ^2 test of an uncertainty of the background normalisation in the data of this size is studied by repeating the χ^2 test on pseudo-data samples from resampling with modified average numbers of background events. In a first calculation, the average numbers of events for all background processes in the pseudo-data samples are varied by +10%. In a sec-

ond calculation they are varied by −10%. The reference distributions are left unchanged.

One can see from the results given in Table 11 that the median χ^2 probability for the channel $H \to W^+W^- \to ll\nu\nu$ is smaller when the average number of background events in the pseudo-data samples is larger than the number assumed for calculating the reference distributions. This is explained by the fact that the signal and background distributions have similar shapes for standard model couplings and a standard model pseudo-data distribution with a larger number of signal or background events can be distinguished from a distribution for anoma-

Fig. 13. Distributions of χ^2 probabilities for the hypothesis of a purely anomalous CP odd coupling. Distributions for disjoint subsamples are shown on the *left* and distributions for pseudo-data samples from resampling are shown on the *right*. For comparison distributions in which background contributions have been neglected are shown in *grey*. The distributions are only shown down to a value of 10^{-15} which is the limit of the numerical precision of the calculation

lous couplings with a higher confidence level. This does not represent a real improvement of the sensitivity of the measurement but a measurement error induced by the error on the background normalisation. If the background in the data is underestimated, the sensitivity for the exclusion of anomalous couplings is slightly overestimated. For the case of less background events the median χ^2 probability increases accordingly. In the $H \to \tau^+\tau^-$ channels this effect is present but very small.

One can see that the median χ^2 probability changes by a factor of less than 1.8 with respect to the case of a correct background prediction. The change in the corresponding number of standard deviations is 0.1 or less in all cases. Thus, the uncertainty on the measured number of back-

ground events in the data has only a small effect on the results of the χ^2 test.

6 Sensitivity to a small CP even anomalous coupling contribution

Once the dominant term of the coupling of a new scalar particle to weak bosons has been determined a question will be whether a small contribution of another coupling term exists. In this section a likelihood fit is used to estimate the sensitivity of the ATLAS experiment to small CP even anomalous couplings that may be present in add-

Table 10. The first two columns show the probabilities for a standard model pseudo-data sample in tests of the hypotheses of purely CP even (CPE) and CP odd (CPO) anomalous couplings to have a χ^2 probability below 5% or $5.7 \times 10^{-7} \hat{=} 5\sigma$. The third and fourth columns show the median χ^2 probabilities and the corresponding deviations from the mean of a Gaussian distribution in standard deviations

| integrated luminosity, hypothesis tested	probability for		median	
	$> 5\sigma$	$< 5\%$	χ^2-prob.	dev. in σ
$H \to W^+W^- \to ll\nu\nu$				
10 fb^{-1} CPE	59%	100%	1.3×10^{-7}	5.3σ
CPO	35%	98%	6.0×10^{-6}	4.5σ
30 fb^{-1} CPE	100%	100%	–	–
CPO	100%	100%	–	–
$H \to \tau^+\tau^-$ combined				
30 fb^{-1} CPE	2%	68%	1.2×10^{-2}	2.5σ
CPO	0%	52%	4.3×10^{-2}	2.0σ

Table 11. Results of the χ^2 test applied to standard model pseudo-data samples from resampling for tests of the hypotheses of purely CP even (CPE) and purely CP odd (CPO) anomalous couplings, with the average numbers of events for all background processes varied by $\pm 10\%$ with respect to the expected numbers. Probabilities for a pseudo-data sample to have a χ^2 probability below 5% or $5.7 \times 10^{-7} \hat{=} 5\sigma$ as well as median χ^2 probabilities and the corresponding deviations from the mean of a Gaussian distribution in standard deviations are given

Results for +10% background events: integrated luminosity, hypothesis tested	probability for		median	
	$> 5\sigma$	$< 5\%$	χ^2-prob.	dev. in σ
$H \to W^+W^- \to ll\nu\nu$				
10 fb^{-1} CPE	61%	100%	7.6×10^{-8}	5.4σ
CPO	37%	98%	4.4×10^{-6}	4.6σ
30 fb^{-1} CPE	100%	100%	–	–
CPO	100%	100%	–	–
$H \to \tau^+\tau^-$ combined				
30 fb^{-1} CPE	3%	68%	1.2×10^{-2}	2.5σ
CPO	0%	52%	4.3×10^{-2}	2.0σ
Results for −10% background events: integrated luminosity, hypothesis tested	$> 5\sigma$	$< 5\%$	χ^2-prob.	dev. in σ
$H \to W^+W^- \to ll\nu\nu$				
10 fb^{-1} CPE	57%	100%	1.7×10^{-7}	5.2σ
CPO	33%	98%	9.1×10^{-6}	4.4σ
30 fb^{-1} CPE	100%	100%	–	–
CPO	100%	100%	–	–
$H \to \tau^+\tau^-$ combined				
30 fb^{-1} CPE	2%	68%	1.3×10^{-2}	2.5σ
CPO	0%	52%	4.3×10^{-2}	2.0σ

ition to the standard model couplings. The likelihood fit is not expected to be sensitive to a contribution by CP odd anomalous couplings in addition to the standard model couplings and hence is not used to determine the sensitivity to a contribution by CP odd couplings. The reason for this expectation will be discussed later in this section.

6.1 Implementation of the likelihood fit

The azimuthal angle between the tagging jets $\Delta\phi_{jj}$ is used as the sensitive quantity in the likelihood fit. In the presence of small CP even anomalous couplings in addition to the standard model couplings the distribution of $\Delta\phi_{jj}$ is
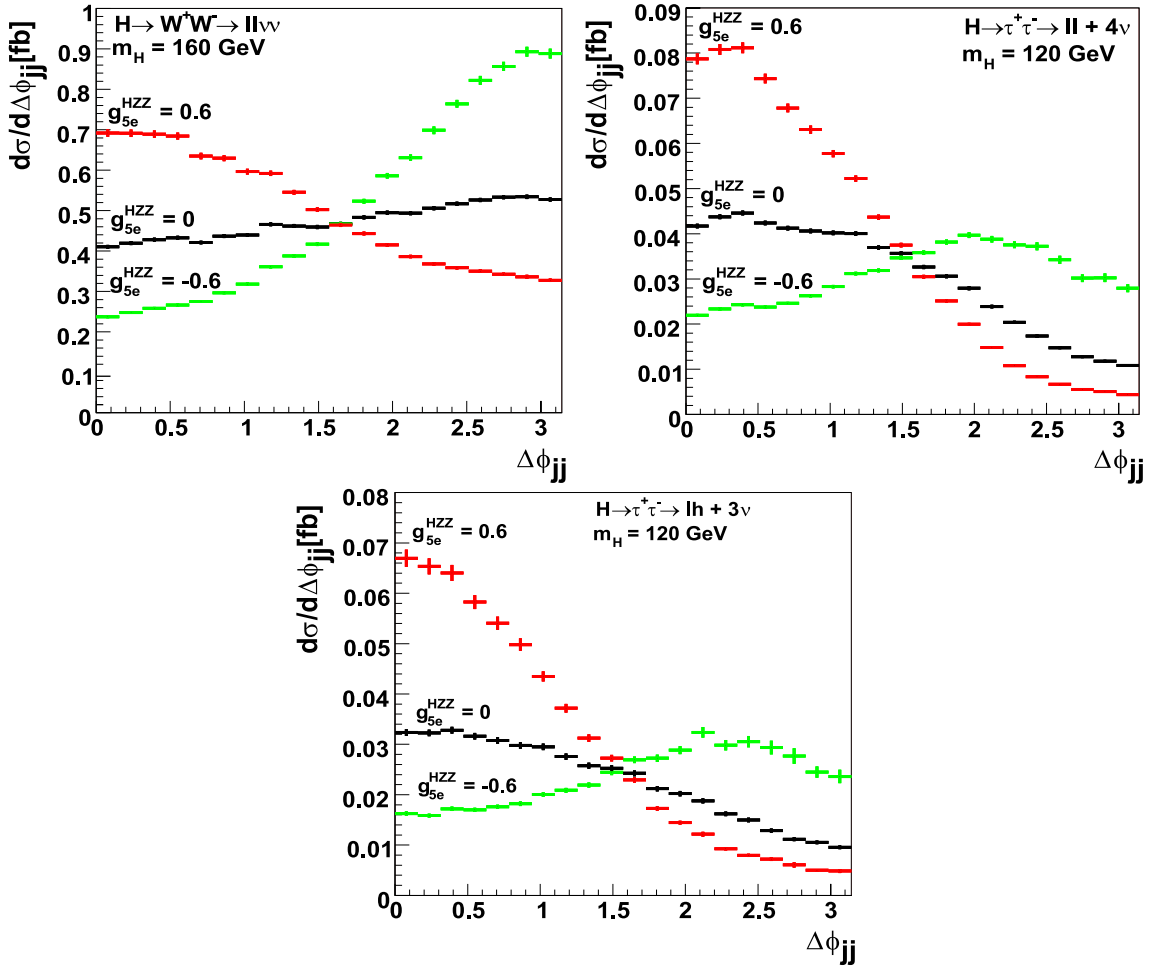
Fig. 14. Distributions of $\Delta\phi_{jj}$ for signal events after all cuts have been applied. For each channel distributions are shown for three different values of the CP even anomalous coupling constant. The distributions were calculated by reweighting of events as described in Sect. 6.2

modified with respect to the standard model case by the interference term in the squared matrix element for Higgs boson production in WBF. Distributions of $\Delta\phi_{jj}$ for signal events with three different values of g_{5e}^{HZZ} are shown in Fig. 14. As before, the ratio of anomalous HWW couplings to anomalous HZZ couplings is kept fixed at $g_{5e}^{HZZ} = g_{5e}^{HWW} / \cos^2\theta_W$. The values of the anomalous coupling constant chosen in Fig. 14 are close to the experimental limits given in Table 3 for the $H \to \tau^+\tau^-$ channels and they are well within the limits for the channel $H \to W^+W^- \to ll\nu\nu$. Furthermore, the values are chosen such that the interference term gives a larger contribution than the squared anomalous term. One can see from Fig. 14 that the interference term is equal to 0 and changes its sign at about $\pi/2$. The maximum of the distribution is located at large or small values of $\Delta\phi_{jj}$ depending on the sign of the anomalous couplings. While the interference term significantly influences the distribution of $\Delta\phi_{jj}$ it has only a small effect on the total cross section due to the asymmetry in the distribution. Thus, it is expected that the sensitivity to a small contribution by CP even anomalous couplings from an analysis of the shape of the distribution of $\Delta\phi_{jj}$ will be higher than from a measurement of the total cross section.

As pointed out in [2] interference effects between the CP odd anomalous couplings and standard model couplings do not show in the shape of the distribution of $\Delta\phi_{jj}$ used in this analysis. Hence, a likelihood fit in the shape of the distribution will probably not be sensitive to small CP odd anomalous couplings. A contribution of the CP odd anomalous couplings may be determined from a measurement of the total cross section. If the contribution is large enough the effect of the squared anomalous matrix element may be observable in the distribution of $\Delta\phi_{jj}$ with the shape as shown in Sect. 5. Recently it has been suggested [24] to use a redefined $\Delta\phi_{jj}$ that can assume positive as well as negative values to study effects of small CP odd anomalous couplings. This is a possible topic for further research extending the analysis presented here.

The logarithm of the likelihood is calculated for the number of bin entries in a pseudo-data histogram n_i, the number of bin entries in a reference histogram ν_i and the number of bins N as

$$\ln L \left(g_{5e}^{HZZ}\right) = \sum_{i=1}^{N} n_i \ln \nu_i \left(g_{5e}^{HZZ}\right). \qquad (24)$$

This form of the likelihood follows from the assumption of a multinomial distribution of the data. The total number of events is not a part of the prediction and the reference histogram is normalised to the data histogram before the likelihood is calculated.

If the total number of events depends on one or more of the arguments of the parameters to be estimated it can be advantageous to include the number of events in the prediction. In this case the distribution of the data is assumed to be given by a product of independent Poisson distributions in each bin. The logarithm of the resulting so-called extended likelihood is given by

$$\ln L \left(g_{5e}^{HZZ} \right) = -\nu_{\text{tot}} \left(g_{5e}^{HZZ} \right) + \sum_{i=1}^{N} n_i \ln \nu_i \left(g_{5e}^{HZZ} \right) \quad (25)$$

with $\nu_{\text{tot}} = \sum \nu_i$. For the calculation of the extended likelihood the reference histogram is normalised to the expected total number of events.

6.2 Reweighting of events

The calculation of the likelihood of (24) and (25) requires reference distributions of $\Delta\phi_{jj}$ for continuous values of the coupling constant g_{5e}^{HZZ}. Instead of generating large event samples for several values of g_{5e}^{HZZ} the reference distributions are calculated by generating a large Monte Carlo event sample with standard model couplings and reweighting the events. Instead of filling histograms with a weight of 1 for each event the events are assigned a weight given by the ratio of the differential cross section at the phase space point of the event with standard model and anomalous couplings to the differential cross section with standard model couplings only. The ratio of the differential cross sections is given by the ratio of the squared matrix element with standard model and anomalous couplings to the squared matrix element with standard model couplings only. If the Monte Carlo event sample with standard model couplings contains enough events to sufficiently populate all regions of phase space that should be populated after the reweighting, all distributions are expected to have the same shape and normalisation as for events generated with anomalous couplings. The only difference expected is that the statistical errors will be different. The statistical error of the sum W of weights w_i in a bin is given by

$$\sigma^2(W) = \sum_i w_i^2 \,, \quad (26)$$

where the sum runs over all events in the bin [25]. If, as expected, all distributions have the correct shape and normalisation, the event selection can be applied as in the case of unweighted events.

The event weights are calculated for the parton momenta in the output files of the program vbfnlo. Subroutines of vbfnlo are used for the calculation of the matrix elements. The method of reweighting is tested by comparing the distributions from reweighted events to the distributions from events that were generated with anomalous

couplings. Distributions at parton level and after the detector simulation and event selection for three different values of g_{5e}^{HZZ} and for all three channels are shown in Fig. 15. One can see from the figure that the distributions from generated and from reweighted events agree with each other both in shape and normalisation. Small differences are observed in the $H \to \tau^+\tau^-$ channels at parton level for large $\Delta\phi_{qq}$.

The correctness of the normalisation of the histograms from reweighted events is explicitly checked in the channel $H \to W^+W^- \to ll\nu\nu$ by comparing the prediction from reweighted events with the prediction from additional event samples that were generated for 6 values of g_{5e}^{HZZ} between -0.9 and 0.9. The calculated total cross section as a function of g_{5e}^{HZZ} is shown in Fig. 16 both at parton level and after the detector simulation and event selection. The values of the cross section at the points of g_{5e}^{HZZ} at which the additional event samples were generated are given in Table 12. One can see from Fig. 16 and Table 12 that within statistical fluctuations the reweighting method leads to the same total cross section prediction as the direct Monte Carlo calculation with anomalous couplings, both at parton level and after the detector simulation and event selection. Furthermore, one can see that the dependence of the total cross section on the anomalous coupling constant g_{5e}^{HZZ} is weaker after the detector simulation and event selection than at parton level. This shows that the reconstruction and selection efficiencies decrease with increasing contribution of the anomalous couplings and it makes the determination of a small anomalous coupling contribution from a measurement of the total cross section difficult.

For the likelihood fit reference distributions of $\Delta\phi_{jj}$ after the detector simulation and event selection are calculated using reweighted events for 2000 equally spaced values of g_{5e}^{HZZ} between -2 and 2. In the regions between those values the histograms are linearly interpolated in each bin. Contributions by background processes are added to the signal distributions with the relative normalisation determined by the cross sections.

6.3 Application to a few individual pseudo-data samples

The likelihood fit is performed on the same standard model Higgs boson pseudo-data samples that were used in Sect. 5. For the $H \to \tau^+\tau^-$ channels the likelihood is calculated in 5 bins. For the channel $H \to W^+W^- \to ll\nu\nu$ 10 bins are used at an integrated luminosity of $10\,\text{fb}^{-1}$ and 20 bins are used at $30\,\text{fb}^{-1}$. Likelihood curves for one pseudo-data sample per channel and integrated luminosity studied are shown in Fig. 17. The results from the $H \to \tau^+\tau^-$ channels are combined by adding the logarithms of the likelihoods. The minima of the likelihood curves and the 1-, 2- and 3σ intervals are given in Table 13.

In the channel $H \to W^+W^- \to ll\nu\nu$ the estimated standard deviation of the parameter g_{5e}^{HZZ} is 0.11 for an integrated luminosity of $30\,\text{fb}^{-1}$. As mentioned in Sect. 2 the normalisation of g_{5e}^{HZZ} is chosen such that a purely anomalous coupling of $g_{5e}^{HWW} = g_{5e}^{HZZ} \cos^2 \theta_w = 1$ roughly
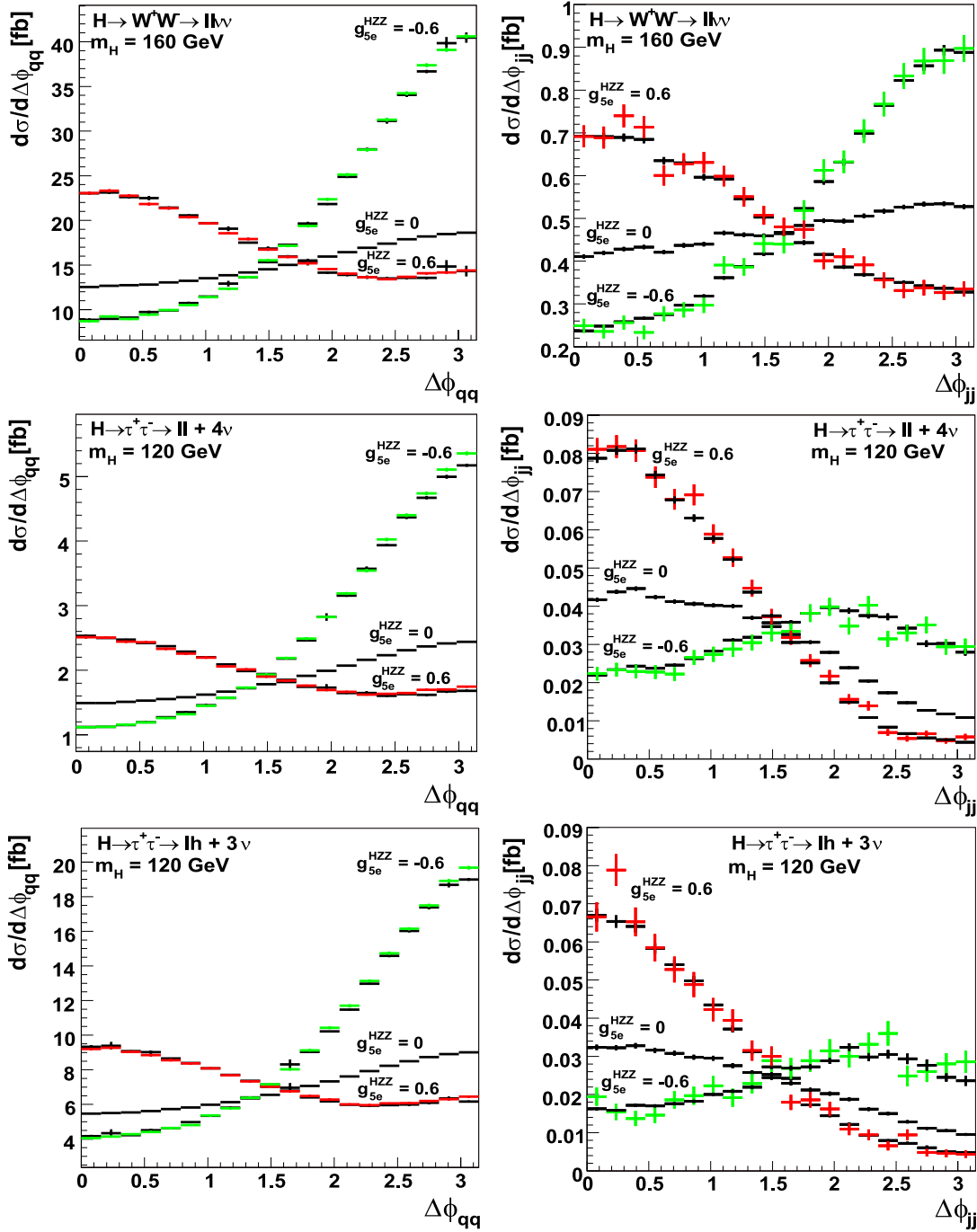
Fig. 15. Distributions from signal events of the azimuthal angle between the scattered quarks at parton level on the *left* and of the azimuthal angle between the tagging jets after the event selection on the *right* for each of the three channels studied and three different values of the anomalous coupling constant g_{5e}^{HZZ}. Distributions calculated by reweighting are shown in *black*. For comparison distributions calculated from events that were generated with anomalous couplings are shown in colour (*dark/light grey*). The coloured (*grey*) distributions are normalised to the cross section for the respective combination of couplings. For the black distributions the number of events is normalised to the standard model cross section while the final normalisation of the histogram follows from the weights

reproduces the standard model cross section in the calculation at $m_H = 120\,\text{GeV}$. For a purely CP even anomalous coupling the same normalisation roughly reproduces the standard model cross section also at $m_H = 160\,\text{GeV}$ in the channel $H \rightarrow W^+W^- \rightarrow ll\nu\nu$. According to the result for the standard deviation it should be possible to reduce the limits on a contribution of the anomalous CP even couplings for a standard model Higgs boson at $m_H = 160\,\text{GeV}$ in the channel $H \rightarrow W^+W^- \rightarrow ll\nu\nu$ by roughly a factor of 6 with respect to the current limits from LEP and L3 given in Table 3 which correspond approximately to a 95% confidence level or about 2σ. An improvement of the current

limits should already be possible for an integrated luminosity of 10 fb^{-1}. In the $H \rightarrow \tau^+\tau^-$ channels at $m_H = 120\,\text{GeV}$ the expected standard deviation corresponds roughly to the current limits for the anomalous CP even HZZ couplings. It should be possible, however, to reduce the limits on the anomalous HWW couplings in these channels. For the anomalous HWW coupling the improvement with respect to the current limits will be larger in all cases since the current limits for this coupling are weaker and the predicted standard deviation for g_{5e}^{HWW} is smaller than that of g_{5e}^{HZZ} by a factor of $\cos^2\theta_w$. However, one should keep in mind that the limits from L3 were determined in sin-
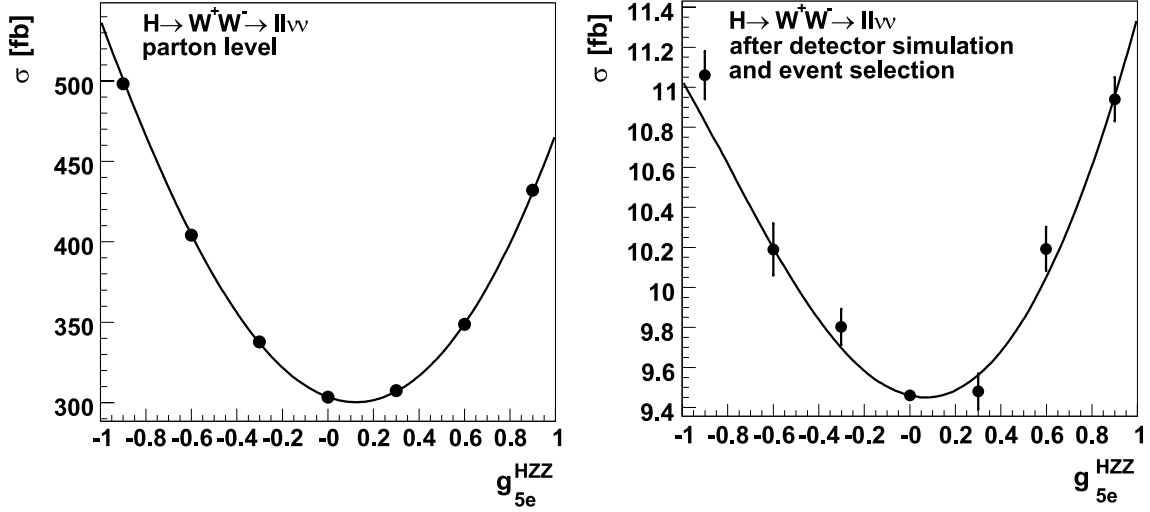
Fig. 16. Total cross section of the signal process in the channel $H \to W^+W^- \to ll\nu\nu$ as a function of the anomalous coupling constant g_{5e}^{HZZ}. The curves were calculated by reweighting of events. The points were calculated from events generated at the respective values of g_{5e}^{HZZ}. The cross section at parton level is shown on the *left* and the cross section after the detector simulation and event selection is shown on the *right*. The errors on the points in the right figure are the binomial errors that arise from the reconstruction and selection efficiencies

Table 12. Values of the total cross section for the signal process in the channel $H \to W^+W^- \to ll\nu\nu$ from reweighted events and for comparison from generated events. Cross section values at parton level are shown on the left and cross section values after the detector simulation and event selection are shown on the right. The statistical errors on the values from generated events at parton level were calculated from the errors given by the program vbfnlo. The statistical errors on the values from reweighting were calculated using the error on the sum of weights from (26). The statistical errors on the values from generated events after the event selection are the binomial errors given by the reconstruction and selection efficiencies

g_{5e}^{HZZ}	σ[fb] at parton level		σ[fb] after ATLFAST and cuts	
	generated	reweighted	generated	reweighted
−0.9	498.4 ± 0.9	499.1 ± 2.3	11.06 ± 0.12	10.82 ± 0.05
−0.6	401.5 ± 0.9	403.0 ± 1.0	10.19 ± 0.13	10.19 ± 0.03
−0.3	335.6 ± 0.9	336.1 ± 0.3	9.80 ± 0.09	9.69 ± 0.02
0.0	303.3	303.3	9.46 ± 0.02	9.46 ± 0.02
0.3	307.3 ± 0.9	307.3 ± 0.2	9.48 ± 0.09	9.57 ± 0.02
0.6	348.6 ± 0.9	350.1 ± 0.7	10.19 ± 0.11	10.06 ± 0.03
0.9	431.4 ± 0.9	432.5 ± 1.5	10.94 ± 0.11	10.97 ± 0.04

gle parameter analyses while in this study both the HWW couplings and the HZZ couplings are varied at the same time.

One can see from Table 13 that the inclusion of the prediction of the total cross section in an extended likelihood fit does not significantly increase the sensitivity in the channel $H \to W^+W^- \to ll\nu\nu$. The effect is larger in the $H \to \tau^+\tau^-$ channels where a reduction of the expected standard deviation by about 15% is observed.

A comparison of the values calculated with background processes taken into account to the values calculated for the signal process only shows that, as expected, the expected sensitivity is lower if background contributions are included. In the $H \to \tau^+\tau^-$ channels the expected stan-

dard deviation increases by about 29% when background contributions are included. In the channel $H \to W^+W^- \to ll\nu\nu$ the predicted standard deviation increases by up to 22%.

6.4 Test of the method using many pseudo-data samples

The properties of the likelihood fit are studied in more detail by applying it to all standard model Higgs boson pseudo-data samples that were used in Sect. 5.3. In this way the standard deviation of the estimated value of g_{5e}^{HZZ} can be directly determined from the distribution of the fit
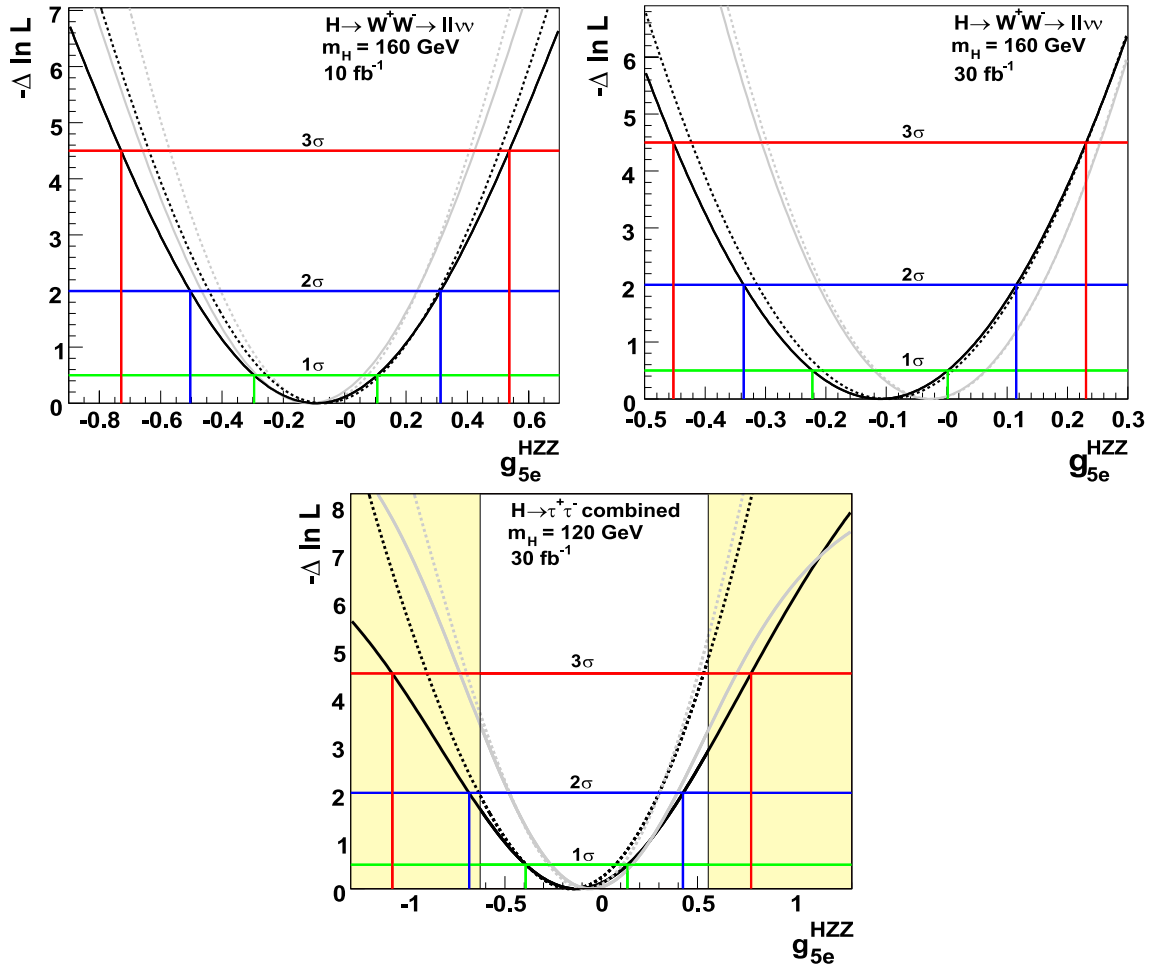
Fig. 17. The logarithm of the likelihood as a function of the anomalous coupling constant g_{5e}^{HZZ} for one pseudo-data sample per channel and integrated luminosity studied. The curves that were calculated with background contributions taken into account are shown in *black*. For comparison, curves that were calculated without considering background processes are shown in *grey*. The *continuous lines* were calculated using the non-extended likelihood. The *dotted lines* were calculated using the extended likelihood. The areas marked in *light yellow (light grey)* are excluded according to the approximate limits at 95% confidence level given in Table 3. 1-, 2-, and 3σ intervals are shown for the case of a non-extended likelihood with background contributions taken into account

results. Furthermore, the distribution of the fit results is used to study the possibility of a bias of the fit method. In addition to the distributions of the fit results pull distributions are calculated with a pull z_i defined as the ratio of the deviation of the fit result m_i from the true value of g_{5e}^{HZZ}, which is 0 for the studied samples, to the standard deviation $\sigma(m_i)$ of the fit result as predicted from the width of the $-\Delta \ln L$ curve:

$$z_i = \frac{m_i}{\sigma(m_i)}. \qquad (27)$$

The pull distributions provide information about the correctness of the estimate of the standard deviation from the $-\Delta \ln L$ curves. If the estimated standard deviation on average is equal to the true standard deviation observed in the distribution of the fit results the pull distribution is expected to follow a normal Gaussian with mean 0 and standard deviation 1 ([26], p. 289f). If the pull distribution has a Gaussian shape with a standard deviation larger

than 1 the error is on average underestimated from the width of the $-\Delta \ln L$ curve, if the standard deviation is smaller than 1 the error from the $-\Delta \ln L$ curve is on average overestimated.

Results are only presented for the pseudo-data samples from resampling as the results for disjoint subsamples are all consistent with the expectations and do not contain any additional information. Distributions of the fit results for the anomalous coupling constant g_{5e}^{HZZ} and pull distributions are shown in Fig. 18 for the non-extended likelihood and in Fig. 19 for the extended likelihood. Gaussian functions are fitted to all distributions and the results for the mean values and standard deviations of the Gaussians are given in Table 14.

The results in Table 14 for the standard deviation of the fit results for g_{5e}^{HZZ} confirm the estimates from the individual likelihood fits in Table 13. In the channel $H \to W^+W^- \to ll\nu\nu$ no statistically significant bias of the fit results is observed. In the $H \to \tau^+\tau^-$ channels the results

Table 13. Results for the parameter g_{5e}^{HZZ} from the likelihood fit for one pseudo-data sample per channel and integrated luminosity studied. Results that have been obtained with background processes taken into account are given in the upper table. Results that have been obtained without considering background contributions are given in the lower table for comparison. For the $H \to \tau^+\tau^-$ case the results for the channel $H \to \tau^+\tau^- \to ll + 4\nu$ and for both $H \to \tau^+\tau^-$ channels combined are given. The estimate of σ is determined by dividing the width of the 1σ interval by 2

background included:	minimum $-\Delta \ln L$	1σ interval	2σ interval	3σ interval	σ estimate
$H \to W^+W^- \to ll\nu\nu$					
10 fb^{-1} non-extended	-0.09	$[-0.30, 0.11]$	$[-0.50, 0.31]$	$[-0.73, 0.54]$	0.20
extended	-0.07	$[-0.26, 0.12]$	$[-0.44, 0.31]$	$[-0.64, 0.51]$	0.19
30 fb^{-1} non-extended	-0.11	$[-0.22, 0.00]$	$[-0.34, 0.12]$	$[-0.45, 0.23]$	0.11
extended	-0.10	$[-0.21, 0.01]$	$[-0.31, 0.12]$	$[-0.42, 0.23]$	0.11
$H \to \tau^+\tau^- \to ll + 4\nu$					
30 fb^{-1} non-extended	-0.25	$[-0.64, 0.12]$	$[-1.23, 0.53]$	$-$	0.38
extended	-0.25	$[-0.59, 0.07]$	$[-0.97, 0.40]$	$[-1.38, 0.74]$	0.33
$H \to \tau^+\tau^-$ combined					
30 fb^{-1} non-extended	-0.13	$[-0.40, 0.13]$	$[-0.69, 0.42]$	$[-1.08, 0.78]$	0.27
extended	-0.16	$[-0.40, 0.06]$	$[-0.64, 0.40]$	$[-0.90, 0, 53]$	0.23

background not included, for comparison:	minimum $-\Delta \ln L$	1σ interval	2σ interval	3σ interval	σ estimate
$H \to W^+W^- \to ll\nu\nu$					
10 fb^{-1} non-extended	-0.11	$[-0.29, 0.06]$	$[-0.47, 0.24]$	$[-0.66, 0.42]$	0.17
extended	-0.08	$[-0.24, 0.07]$	$[-0.40, 0.24]$	$[-0.57, 0.41]$	0.16
30 fb^{-1} non-extended	-0.03	$[-0.12, 0.06]$	$[-0.21, 0.16]$	$[-0.31, 0.25]$	0.09
extended	-0.03	$[-0.12, 0.07]$	$[-0.21, 0.16]$	$[-0.30, 0.25]$	0.09
$H \to \tau^+\tau^- \to ll + 4\nu$					
30 fb^{-1} non-extended	-0.27	$[-0.55, 0.00]$	$[-0.89, 0.27]$	$[-1.89, 0.61]$	0.28
extended	-0.27	$[-0.54, -0.01]$	$[-0.86, 0.26]$	$[-1.25, 0.55]$	0.27
$H \to \tau^+\tau^-$ combined					
30 fb^{-1} non-extended	-0.06	$[-0.27, 0.15]$	$[-0.48, 0, 40]$	$[-0.73, 0.71]$	0.21
extended	-0.09	$[-0.28, 0.10]$	$[-0.49, 0.30]$	$[-0.70, 0.50]$	0.19

show small statistically significant biases which are attributed to deviations of the distributions from the Gaussian shape which can be seen in Fig. 18 and to a lesser degree in Fig. 19. The bias, while statistically significant, is smaller than 4% of the expected standard deviation in each case. The standard deviations of the pull distributions are compatible with 1 within statistical fluctuations for the channel $H \to W^+W^- \to ll\nu\nu$ and an integrated luminosity of 30 fb^{-1}. The standard deviations in this channel for 10 fb^{-1} and in the $H \to \tau^+\tau^-$ channels are slightly smaller than 1 which indicates that the errors are overestimated from the $-\Delta \ln L$ curves by a small factor in these cases.

6.5 Effects of uncertainties on the number of background events

The effects of an uncertainty on the measured number of background events of $\pm 10\%$ on the results of the likelihood fit are studied as for the χ^2 test (see Sect. 5.4) by repeating the likelihood fit on pseudo-data samples in which the average number of events for all background processes is varied by $+10\%$ and repeating it again for pseudo-data samples in which the average number of events for all background processes is varied by -10%.

One can see from the results given in Tables 15 and 16 that a variation of the number of background events introduces a bias in the fit and a small change in the standard deviation of the fit results. The bias is larger than the change in the standard deviation in most cases and of similar size in others. The bias is negative if there are more background events in the data than assumed and positive if there are less background events.

For the $W \to W^+W^- \to ll\nu\nu$ channel the bias in the extended likelihood fit is larger than in the non-extended likelihood fit whereas for the $H \to \tau^+\tau^-$ channels the bias in the non-extended likelihood fit is larger. The total uncertainty on the fit result for g_{5e}^{HZZ} for a single data sample induced by a variation of the number of background events of $\pm 10\%$ is approximately ± 0.02.
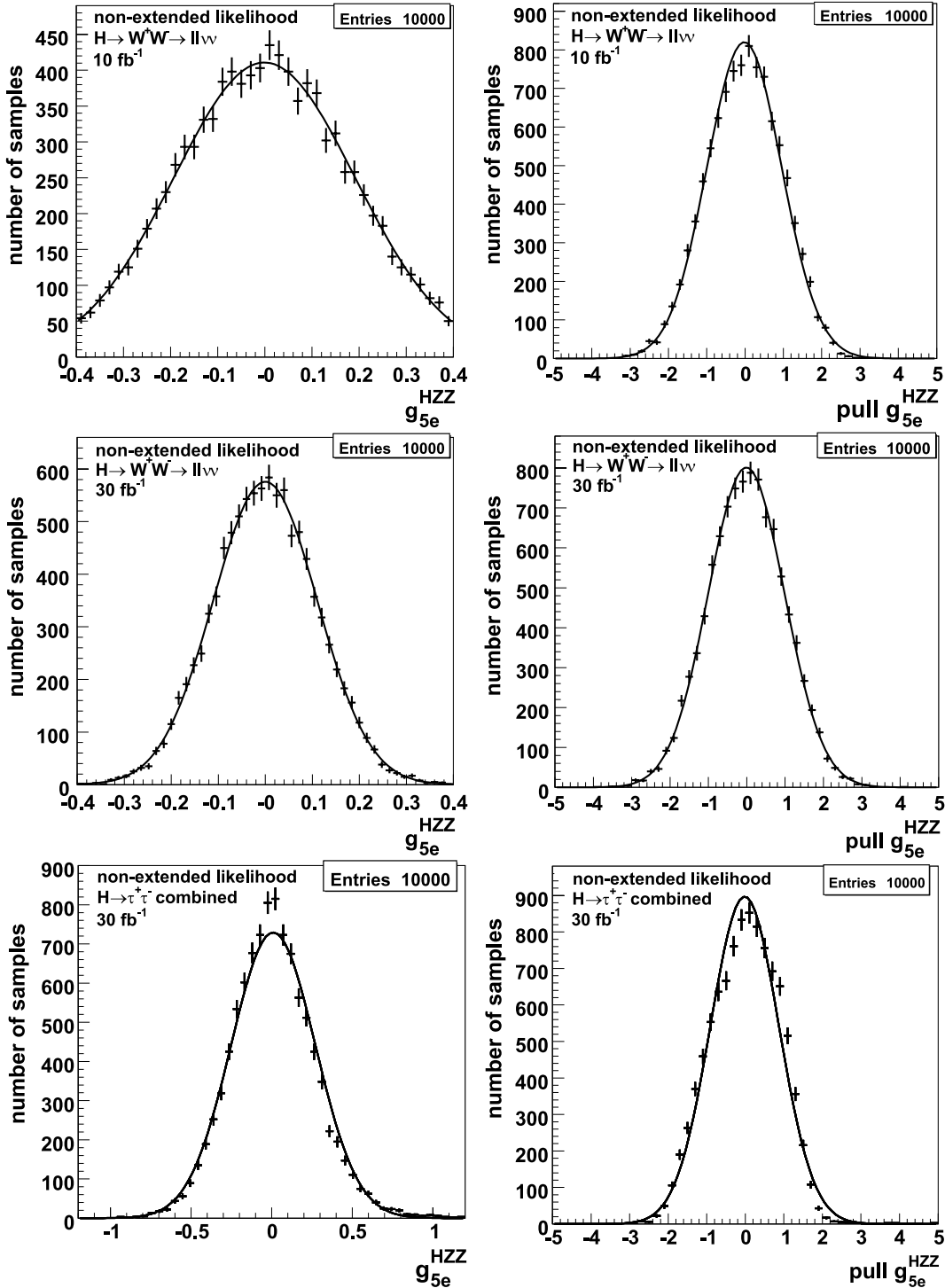
Fig. 18. Distributions of the results of the non-extended likelihood fit for g_{5e}^{HZZ} are shown on the *left* and the corresponding pull distributions are shown on the *right*. Gaussian functions that were fitted to all distributions are also shown

7 Summary

The prospects for the measurement of the structure of the Higgs boson coupling to two weak gauge bosons in the weak boson fusion channel are studied using the fast simulation of the ATLAS detector. The distribution of the azimuthal angles between the tagging jets $\Delta\phi_{jj}$ after an event selection optimised for maximum discovery potential is used in the analysis which is performed for the

Higgs boson decay channels $H \to \tau^+\tau^- \to ll + 4\nu$ and $H \to \tau^+\tau^- \to lh + 3\nu$ at $m_H = 120\,\text{GeV}$ and $H \to W^+W^- \to ll\nu\nu$ at $m_H = 160\,\text{GeV}$.

In addition to the standard model vertex which is proportional to $g^{\mu\nu}$ additional tensor vertices which follow from terms of dimension 6 in an effective Lagrangian are studied. The coupling terms differ in their properties under CP transformations. Under the assumption of CP invariance the determination of the dominant coupling term permits the de-
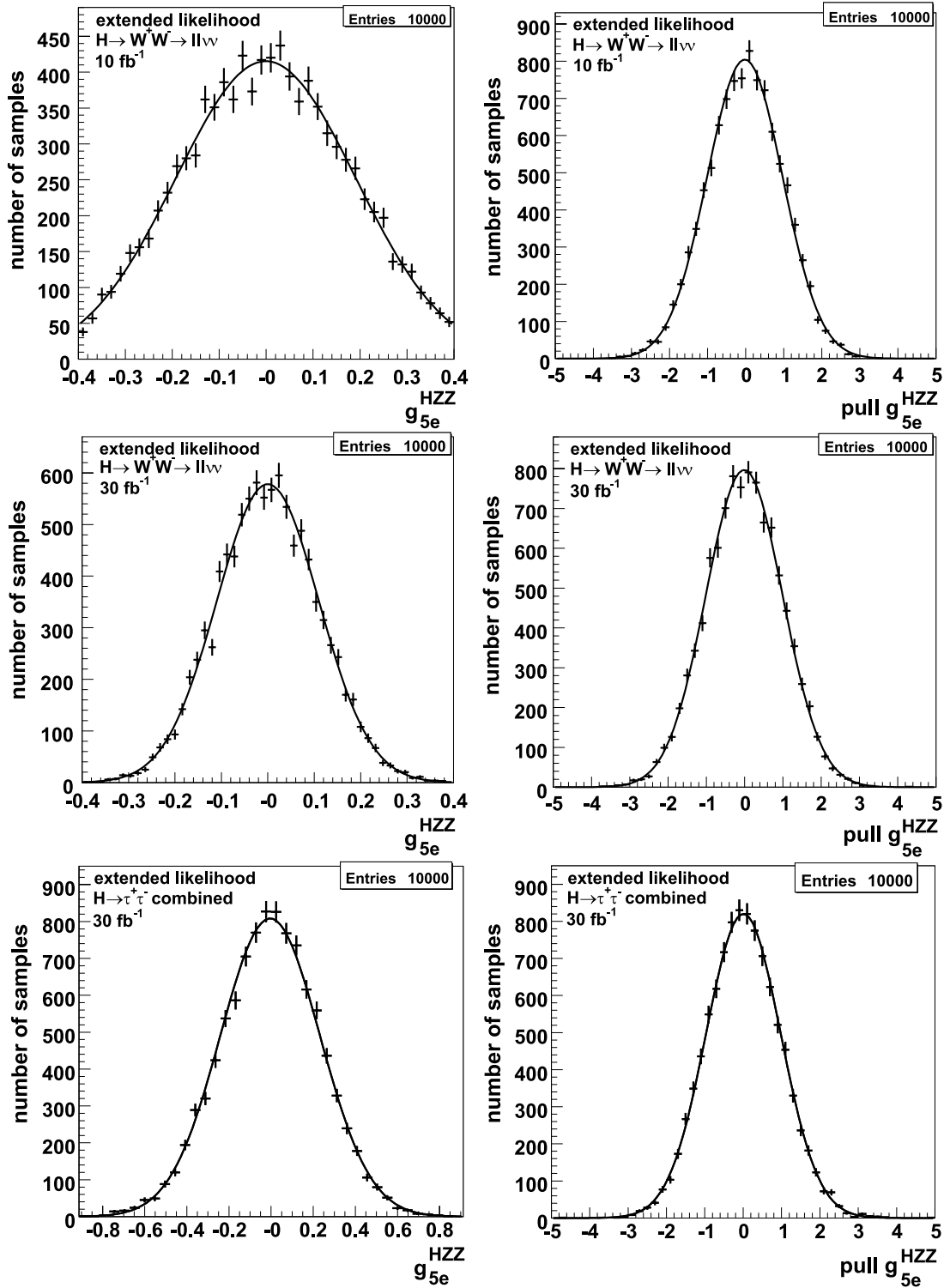
Fig. 19. Distributions of the results of the extended likelihood fit for g_{5e}^{HZZ} are shown on the *left* and the corresponding pull distributions are shown on the *right*. Gaussian functions that were fitted to all distributions are also shown

termination of the CP quantum number of the Higgs boson. The ratio of anomalous HWW couplings to anomalous HZZ couplings was fixed for simplicity to $g_{5e}^{HWW}/g_{5e}^{HZZ} = \cos^2\theta_w$. It is shown that it should be possible with the ATLAS detector to exclude the possibility of a purely anomalous CP even or a purely anomalous CP odd coupling at a confidence level corresponding to approximately 5σ for a standard model Higgs boson at $m_H = 160\,\text{GeV}$ from the

analysis in the channel $H \to W^+W^- \to ll\nu\nu$ for low luminosity data corresponding to an integrated luminosity of $10\,\text{fb}^{-1}$. For a standard model Higgs boson at $m_H = 120\,\text{GeV}$ an exclusion with a confidence level corresponding to 2σ or more is considered possible from the analysis in the $H \to \tau^+\tau^-$ channels for an integrated luminosity of $30\,\text{fb}^{-1}$. If the confidence level observed for one anomalous coupling (CP even or CP odd) is lower than the stated values it is expected

Table 14. Results of Gaussian fits to the distributions of fit results for g_{5e}^{HZZ} are given in the upper table. Results of Gaussian fits to the pull distributions are given in the lower table. The distributions were calculated by applying the likelihood fit to the pseudo-data samples from resampling as described in the text

| | | distributions of the fit results for g_{5e}^{HZZ} for pseudo-data samples from resampling | |
		mean	σ
$H \rightarrow W^+W^- \rightarrow ll\nu\nu$			
10 fb^{-1}	non-extended	$(-0.8 \pm 2.2) \times 10^{-3}$	0.1932 ± 0.0021
	extended	$(-0.7 \pm 2.2) \times 10^{-3}$	0.1921 ± 0.0021
30 fb^{-1}	non-extended	$(-0.1 \pm 1.1) \times 10^{-3}$	0.11084 ± 0.00080
	extended	$(0.0 \pm 1.1) \times 10^{-3}$	0.11039 ± 0.00079
$H \rightarrow \tau^+\tau^-$ combined			
30 fb^{-1}	non-extended	$(1.01 \pm 0.28) \times 10^{-2}$	0.2612 ± 0.0019
	extended	$(-0.46 \pm 0.24) \times 10^{-2}$	0.2372 ± 0.0017
		pull distributions for pseudo-data samples from resampling	
		mean	σ
$H \rightarrow W^+W^- \rightarrow ll\nu\nu$			
10 fb^{-1}	non-extended	$(-2.0 \pm 0.97) \times 10^{-2}$	0.9728 ± 0.0069
	extended	$(-1.96 \pm 0.99) \times 10^{-2}$	0.9915 ± 0.0070
30 fb^{-1}	non-extended	$(-1.0 \pm 1.0) \times 10^{-2}$	0.9954 ± 0.0070
	extended	$(-1.1 \pm 1.0) \times 10^{-2}$	1.0012 ± 0.0071
$H \rightarrow \tau^+\tau^-$ combined			
30 fb^{-1}	non-extended	$(-1.66 \pm 0.89) \times 10^{-2}$	0.8875 ± 0.0063
	extended	$(0.56 \pm 0.97) \times 10^{-2}$	0.9727 ± 0.0069

Table 15. Results of the likelihood fit to pseudo-data samples from resampling with the average number of events for all background processes varied by $+10\%$ with respect to the expected number. Results of Gaussian fits to the distributions of fit results for g_{5e}^{HZZ} are given in the upper table. Results of Gaussian fits to the pull distributions are given in the lower table

Results for +10% background events:

| | | distributions of the fit results for g_{5e}^{HZZ} for pseudo-data samples from resampling | |
		mean	σ
$H \rightarrow W^+W^- \rightarrow ll\nu\nu$			
10 fb^{-1}	non-extended	$(-8.1 \pm 2.1) \times 10^{-3}$	0.1872 ± 0.0019
	extended	$(-1.15 \pm 0.22) \times 10^{-2}$	0.1927 ± 0.0021
30 fb^{-1}	non-extended	$(-6.2 \pm 1.1) \times 10^{-3}$	0.11000 ± 0.00079
	extended	$(-9.7 \pm 1.1) \times 10^{-3}$	0.11360 ± 0.00082
$H \rightarrow \tau^+\tau^-$ combined			
30 fb^{-1}	non-extended	$(-9.3 \pm 2.6) \times 10^{-3}$	0.2594 ± 0.0018
	extended	$(-1.00 \pm 0.26) \times 10^{-2}$	0.2557 ± 0.0018
		pull distributions for pseudo-data samples from resampling	
		mean	σ
$H \rightarrow W^+W^- \rightarrow ll\nu\nu$			
10 fb^{-1}	non-extended	$(-4.89 \pm 0.96) \times 10^{-2}$	0.9642 ± 0.0068
	extended	$(-6.5 \pm 1.0) \times 10^{-2}$	1.0006 ± 0.0071
30 fb^{-1}	non-extended	$(-6.5 \pm 1.0) \times 10^{-2}$	1.0015 ± 0.0071
	extended	$(-9.8 \pm 1.0) \times 10^{-2}$	1.0256 ± 0.0073
$H \rightarrow \tau^+\tau^-$ combined			
30 fb^{-1}	non-extended	$(-8.53 \pm 0.91) \times 10^{-2}$	0.9051 ± 0.0064
	extended	$(-1.0 \pm 1.0) \times 10^{-2}$	1.0150 ± 0.0072

Table 16. Results of the likelihood fit to pseudo-data samples from resampling with the average number of events for all background processes varied by -10% with respect to the expected number. Results of Gaussian fits to the distributions of fit results for g_{5e}^{HZZ} are given in the upper table. Results of Gaussian fits to the pull distributions are given in the lower table

Results for -10% background events:		distributions of the fit results for g_{5e}^{HZZ} for pseudo-data samples from resampling	
		mean	σ
$H \to W^+W^- \to ll\nu\nu$			
$10\,\mathrm{fb}^{-1}$	non-extended	$(4.6 \pm 2.2) \times 10^{-3}$	0.1909 ± 0.0019
	extended	$(8.4 \pm 2.1) \times 10^{-3}$	0.1844 ± 0.0019
$30\,\mathrm{fb}^{-1}$	non-extended	$(5.5 \pm 1.1) \times 10^{-3}$	0.11279 ± 0.00081
	extended	$(9.4 \pm 1.1) \times 10^{-3}$	0.10814 ± 0.00077
$H \to \tau^+\tau^-$ combined			
$30\,\mathrm{fb}^{-1}$	non-extended	$(2.84 \pm 0.27) \times 10^{-2}$	0.2686 ± 0.0019
	extended	$(-1.6 \pm 2.3) \times 10^{-3}$	0.2313 ± 0.0016
		pull distributions for pseudo-data samples from resampling	
		mean	σ
$H \to W^+W^- \to ll\nu\nu$			
$10\,\mathrm{fb}^{-1}$	non-extended	$(1.31 \pm 0.96) \times 10^{-2}$	0.9565 ± 0.0068
	extended	$(3.38 \pm 0.96) \times 10^{-2}$	0.9601 ± 0.0068
$30\,\mathrm{fb}^{-1}$	non-extended	$(4.0 \pm 1.0) \times 10^{-2}$	0.9961 ± 0.0070
	extended	$(7.50 \pm 0.99) \times 10^{-2}$	0.9854 ± 0.0070
$H \to \tau^+\tau^-$ combined			
$30\,\mathrm{fb}^{-1}$	non-extended	$(4.33 \pm 0.89) \times 10^{-2}$	0.8917 ± 0.0064
	extended	$(1.50 \pm 0.96) \times 10^{-2}$	0.9613 ± 0.0068

that the confidence level for the other anomalous coupling will be higher. An uncertainty of $\pm 10\%$ on the measured number of background events is shown to have only a small effect on the expected exclusion limits.

The sensitivity of the ATLAS experiment to a small anomalous CP even coupling present *in addition* to the standard model coupling is studied using a likelihood fit. The standard deviation of the measured anomalous coupling constant g_{5e}^{HZZ} for the case of a standard model Higgs boson at $m_H = 160\,\mathrm{GeV}$ in the channel $H \to W^+W^- \to ll\nu\nu$ is estimated to be 0.11 for an integrated luminosity of $30\,\mathrm{fb}^{-1}$ and 0.19 for an integrated luminosity of $10\,\mathrm{fb}^{-1}$. The normalisation of g_{5e}^{HZZ} is chosen such that a value for g_{5e}^{HZZ} of $1/cos^2\theta_w$ roughly gives the standard model cross section in a calculation with a purely anomalous coupling. A measurement of a contribution of an anomalous coupling of 0 and a standard deviation as estimated for an integrated luminosity of $30\,\mathrm{fb}^{-1}$ would correspond to an improvement of the current experimental limits from measurements at LEP and especially the L3 experiment by roughly a factor of 6. The results given were determined using only the shape of the $\Delta\phi_{jj}$ distribution. The inclusion of the prediction of the total cross section in an extended likelihood fit gives practically no advantage. No statistically significant bias is observed in distributions of the fit results for many Monte Carlo event samples.

For a standard model Higgs boson at $m_H = 120\,\mathrm{GeV}$ in the $H \to \tau^+\tau^-$ channels a standard deviation of 0.26 from a non-extended likelihood fit using the shape of the $\Delta\phi_{jj}$ distribution alone and 0.24 from an extended likelihood fit is expected for an integrated luminosity of $30\,\mathrm{fb}^{-1}$. For the anomalous HZZ coupling this result corresponds roughly to the current experimental limits while it would permit an improvement of the limits for the anomalous HWW coupling. Distributions of the fit results show small deviations from the Gaussian shape and a small statistically significant bias is observed in the fit results for these channels.

It is shown that an uncertainty of $\pm 10\%$ on the number of background events in the data leads to an uncertainty of roughly ± 0.02 on the fit results in both decay channels of the Higgs boson.

7.1 Concluding Remarks

The effects of the emission of an additional gluon on the $\Delta\phi_{jj}$ distribution in the weak boson fusion process have been studied in [5]. It was found that the changes to the distribution in a next-to-leading order QCD calculation are very small and no significant effect on the results of this study is expected from those corrections to the signal process.

Recently it has been shown [24] that it is possible to observe interference effects between CP even and CP odd couplings by using a different definition of the azimuthal angle between the tagging jets. Instead of using the absolute value of the angle, as was done in this study, the sign of the angle is defined with respect to the direction of the tagging jet in one arbitrarily fixed detector hemisphere. The prospects for the measurement with the ATLAS detector of a CP odd coupling contribution in addition to standard model and/or CP even anomalous couplings using the redefined azimuthal angle difference are possible topics for further research.

Version 10.0.1 of ATHENA was used. The version of ATLFAST used in ATHENA 10.0.1 has not been formally validated within the ATLAS collaboration and, albeit being considered as appropriate for this study, results obtained using this version cannot be compared directly to other ATLAS results.

References

1. S. Asai et al., Eur. Phys. J. C **32**, 19 (2004)
2. T. Plehn, D. Rainwater, D. Zeppenfeld, Phys. Rev. Lett. **88**, 051 801 (2002) [hep-ph/0105325]
3. C. Ruwiedel, Studie zur Messbarkeit der Struktur der Kopplung eines Higgs-Bosons an schwache Eichbosonen in der Vektorbosonfusion mit dem ATLAS-Detektor am LHC, Diplomarbeit, BONN-IB-2006-06
4. W. Buchmüller, D. Wyler, Nucl. Phys. B **268**, 621 (1986)
5. T. Figy, D. Zeppenfeld, Phys. Lett. B **591**, 297 (2004) [hep-ph/0403297]
6. L3 Collaboration, P. Achard et al., Phys. Lett. B **589**, 89 (2004) [hep-ex/0403037]
7. E. Boos et al., hep-ph/0109068
8. T. Sjöstrand et al., Comput. Phys. Commun. **135**, 238 (2001) [hep-ph/0010017]
9. S. Jadach, Z. Was, R. Decker, J.H. Kuehn, Comput. Phys. Commun. **76**, 361 (1993)
10. E. Barberio, Z. Was, Comput. Phys. Commun. **79**, 291 (1994)
11. E. Richter-Was, D. Froidevaux, L. Poggioli, ATLFAST 2.0, a fast simulation package for ATLAS, ATL-PHYS-98-131
12. H.L. Lai et al., Eur. Phys. J. C **12**, 375 (2000) [hep-ph/9903282]
13. D. Zeppenfeld et al., provided by the auther via e-mail
14. D. Zeppenfeld, private communication
15. S.R. Slabospitsky, L. Sonnenschein, Comput. Phys. Commun. **148**, 87 (2002) [hep-ph/0201292]
16. F. Maltoni, T. Stelzer, JHEP **0302**, 027 (2003) [hep-ph/0208156]
17. H. Hagiwara, D. Zeppenfeld, Nucl. Phys. B **313**, 560 (1989)
18. H. Chehime, D. Zeppenfeld, Phys. Rev. D **47**, 3898 (1993)
19. Particle Data Group, Phys. Lett. B **592**, 1 (2004)
20. ATLAS Collaboration, O.B. Abdinov et al., ATLAS detector and physics performance, Technical Design Report, CERN/LHCC/99-14 and CERN/LHCC/99-15
21. Michael Heldmann, private communication
22. R. Barlow, Resampling and the Bootstrap, SLUO Lecture on Statistics and Numerical Methods in HEP, http://www.hep.man.ac.uk/u/roger/
23. LEP Collaborations ALEPH, DELPHI, L3, OPAL, LEP Electroweak Working Group, hep-ex/0511027
24. V. Hankele, G. Klämke, D. Zeppenfeld, T. Figy, hep-ph/0609075
25. R. Barlow, J. Comput. Phys. **72**, 202 (1987)
26. A.G. Frodesen, O. Skjeggestad, H. Tøfte, Probability and Statistics in Particle Physics, Universitetsforlaget, Oslo (1979)